

Effective Regularization Through Loss-Function Metalearning

SANTIAGO GONZALEZ*, University of Texas at Austin, USA and Cognizant AI Labs, USA
RISTO MIIKKULAINEN, University of Texas at Austin, USA and Cognizant AI Labs, USA

Evolutionary optimization, such as the TaylorGLO method, can be used to discover novel, customized loss functions for deep neural networks, resulting in improved performance, faster training, and improved data utilization. A likely explanation is that such functions discourage overfitting, leading to effective regularization. This paper demonstrates theoretically that this is indeed the case for TaylorGLO: Decomposition of learning rules makes it possible to characterize the training dynamics and show that the loss functions evolved by TaylorGLO balance the pull to zero error, and a push away from it to avoid overfitting. They may also automatically take advantage of label smoothing. This analysis leads to an invariant that can be utilized to make the metalearning process more efficient in practice; the mechanism also results in networks that are robust against adversarial attacks. Loss-function evolution can thus be seen as a well-founded new aspect of metalearning in neural networks.

CCS Concepts: • **Computing methodologies** → **Machine learning algorithms**; Distributed algorithms; *Computer vision*; **Genetic algorithms**; **Neural networks**.

Additional Key Words and Phrases: Deep Learning, Neural Networks, Regularization, Loss Functions, Metalearning, Evolutionary Computation

ACM Reference Format:

Santiago Gonzalez and Risto Miikkulainen. 2021. Effective Regularization Through Loss-Function Metalearning. 1, 1 (October 2021), 27 pages.

1 INTRODUCTION

Regularization is a key concept in deep learning: It guides learning towards configurations that are likely to perform robustly on unseen data. Different regularization approaches originate from intuitive understanding of the learning process and have been shown to be effective empirically. However, the understanding of the underlying mechanisms, the different types of regularization, and their interactions, is limited.

Recently, loss function optimization has emerged as a new area of metalearning, and shown great potential in training better models. Experiments suggest that evolved loss functions serve as regularizers in a surprising but transparent way: They prevent the network from learning too confident predictions [e.g. Baikal loss; Gonzalez and Miikkulainen 2020]. While it may be too early to develop a comprehensive theory of regularization, it may be possible to make progress in understanding regularization of this specific type. That is the goal of this paper.

Since metalearned loss functions are customized to a given architecture-task pair, there needs to be a shared framework under which loss functions can be analyzed and compared. The TaylorGLO [Gonzalez and Miikkulainen 2021] technique for loss function metalearning lends itself well to such analysis: It represents loss functions as multivariate Taylor polynomials, and leverages evolution to optimize a fixed number of parameters in this representation. In this framework, the SGD learning

*Current affiliation: Apple Inc.

Authors' addresses: Santiago Gonzalez, University of Texas at Austin, Austin, Texas, USA and Cognizant AI Labs, San Francisco, California, USA, slgonzalez@utexas.edu; Risto Miikkulainen, University of Texas at Austin, Austin, Texas, USA and Cognizant AI Labs, San Francisco, California, USA, risto@cs.utexas.edu.

rule is decomposed to coefficient expressions that can be defined for a wide range of loss functions. These expressions provide an intuitive understanding of the training dynamics in specific contexts.

Using this framework in this paper, mean squared error (MSE), cross-entropy, Baikal, and TaylorGLO loss functions are analyzed at the null epoch, when network weights are similarly distributed, and in a zero training error regime, where the training samples' labels have been perfectly memorized. For any intermediate point in the training process, the strength of the zero training error regime as an attractor is analyzed and a constraint on this property is derived on TaylorGLO parameters by characterizing how the output distribution's entropy changes. In a concrete TaylorGLO loss function that has been metalearned, these attraction dynamics are calculated for individual samples at every epoch in a real training run, and contrasted with those for the cross-entropy loss. This comparison provides clarity on how TaylorGLO avoids becoming overly confident in its predictions. Further, the analysis shows how label smoothing [Szegedy et al. 2016], a traditional type of regularization, can be implicitly encoded by TaylorGLO loss functions: Any representable loss function has label-smoothed variants that are also representable by the parameterization.

From these analyses, practical opportunities arise. First, at the null epoch, where the desired behavior can be characterized clearly, an invariant can be derived on a TaylorGLO loss function's parameters that must hold true for networks to be trainable. This constraint is then applied within the TaylorGLO algorithm to guide the search process towards good loss functions more efficiently. Second, loss-function-based regularization results in robustness that should e.g. make them more resilient to adversarial attacks. This property is demonstrated experimentally by incorporating adversarial robustness as an objective within the TaylorGLO search process. Thus, loss-function metalearning can be seen as a well-founded and practical approach to effective regularization in deep learning.

2 BACKGROUND

Regularization traditionally refers to methods for encouraging smoother mappings by adding a regularizing term to the objective function, i.e., to the loss function in neural networks. It can be defined more broadly, however, e.g. as "any modification we make to a learning algorithm that is intended to reduce its generalization error but not its training error" [Goodfellow et al. 2015]. To that end, many regularization techniques have been developed that aim to improve the training process in neural networks. These techniques can be architectural in nature, such as Dropout [Srivastava et al. 2014] and Batch Normalization [Ioffe and Szegedy 2015], or they can alter some aspect of the training process, such as label smoothing [Szegedy et al. 2016] or the minimization of a weight norm [Hanson and Pratt 1989]. These techniques are briefly reviewed in this section, providing context for loss-function metalearning.

2.1 Implicit biases in optimizers

It may seem surprising that overparameterized neural networks are able to generalize at all, given that they have the capacity to memorize a training set perfectly, and in fact sometimes do (i.e., zero training error is reached). Different optimizers have different implicit biases that determine which solutions are ultimately found. These biases are helpful in providing implicit regularization to the optimization process [Neyshabur et al. 2015]. Such implicit regularization is the result of a network norm—a measure of complexity—that is minimized as optimization progresses. This is why models continue to improve even after training set has been memorized (i.e., the training error global optima is reached) [Neyshabur et al. 2017].

For example, the process of stochastic gradient descent (SGD) itself has been found to provide regularization implicitly when learning on data with noisy labels [Blanc et al. 2020]. In overparameterized networks, adaptive optimizers find very different solutions than basic SGD. These solutions tend to have worse generalization properties, even though they tend to have lower training errors [Wilson et al. 2017].

2.2 Regularization approaches

While optimizers may minimize a network norm implicitly, regularization approaches supplement this process and make it explicit. For example, a common way to restrict the parameter norm explicitly is through weight decay. This approach discourages network complexity by placing a cost on weights [Hanson and Pratt 1989].

Generalization and regularization are often characterized at the end of training, i.e. as a behavior that results from the optimization process. Various findings have influenced work in regularization. For example, flat landscapes have better generalization properties [Chaudhari et al. 2019; Keskar et al. 2017; Li et al. 2018]. In overparameterized cases, the solutions at the center of these landscapes may have zero training error (i.e., perfect memorization), and under certain conditions, zero training error empirically leads to lower generalization error [Belkin et al. 2019; Nakkiran et al. 2019]. However, when a training loss of zero is reached, generalization suffers [Ishida et al. 2020]. This behavior can be thought of as overtraining, and techniques have been developed to reduce it at the end of the training process, such as early stopping [Morgan and Boulard 1990] and flooding [Ishida et al. 2020].

Both flooding and early stopping assume that overfitting happens at the end of training, which is not always true [Golatkar et al. 2019]. In fact, the order in which easy-to-generalize and hard-to-generalize concepts are learned is important for the network’s ultimate generalization. For instance, larger learning rates early in the training process often lead to better generalization in the final model [Li et al. 2019]. Similarly, low-error solutions found by SGD in a relatively quick manner—such as through high learning rates—often have good generalization properties [Yao et al. 2007].

Other techniques tackle overfitting by making it more difficult. Dropout [Srivastava et al. 2014] makes some connections disappear. Cutout [DeVries and Taylor 2017], Mixup [Zhang et al. 2018], and their composition, CutMix [Yun et al. 2019], augment training data with a broader variation of examples.

Notably, regularization is not a one-dimensional continuum. Different techniques regularize in different ways that often interact. For example, flooding invalidates performance gains from early stopping [Ishida et al. 2020]. However, ultimately all regularization techniques alter the gradients that result from the training loss. This observation suggests loss-function optimization might be an effective way to regularize the training process.

2.3 General loss-function metalearning

The idea of metalearning loss-functions has a long history, with many promising recent developments in practical settings.

Prior work in reinforcement learning showed that metalearning various types of objectives is useful. For instance, in evolving policy gradients [Houthoofd et al. 2018], the policy loss is not represented symbolically, but rather as a neural network that convolves over a temporal sequence of context vectors. In reward function search [Niekum et al. 2010], the task is framed as a genetic programming problem, leveraging PushGP [Spector et al. 2001]. Various actor-critic reinforcement learning approaches have tackled learning a meta-critic neural network that can generate losses

[Sung et al. 2017; Zhou et al. 2020]. Metalearned critic network techniques have also been applied outside of reinforcement learning to train better few-shot classifiers [Antoniou and Storkey 2019].

In unsupervised representation learning, weight update rules for semi-supervised learning have themselves been metalearned successfully [Metz et al. 2018]. The update rules were constrained to fit a biological neuron model and transferred well between tasks.

2.4 Loss-function metalearning for deep networks: GLO and TaylorGLO

Concrete loss-function metalearning for deep networks was first introduced by Gonzalez and Miikkulainen [2020] as an automatic way to find customized loss functions that optimize a performance metric for a model. The technique, a genetic programming approach named GLO, discovered one particular loss function, Baikal, that improves classification accuracy, training speed, and data utilization. Intuitively, Baikal achieved these properties through a form of regularization that ensured the model would not become overly confident in its predictions. That is, instead of monotonically decreasing the loss when the output gets closer to the correct value, Baikal loss increases rapidly when the output is almost correct, thus discouraging extreme accuracy. This paper shows how training dynamics are specifically impacted in this manner when training with the Baikal loss.

Overall, GLO demonstrated that while learned loss functions’ generalization effects transfer across datasets and models to some extent, they are most powerful when they are customized to individual tasks and architectures. Different loss functions can take advantage of the different characteristics of each such setting. Other techniques have advanced this new field further, for example by metalearning state-dependent loss functions for inverse dynamics models [Morse et al. 2020], and using a trained network that is itself a metalearned loss function [Bechtle et al. 2019].

One particular technique, TaylorGLO [Gonzalez and Miikkulainen 2021], lends itself well to analyzing what makes loss-function metalearning effective. TaylorGLO represents loss functions as parameterizations of multivariate Taylor polynomials. This parameterization allows it to scale to models with millions of trainable parameters, including a variety of deep learning architectures in image classification tasks. TaylorGLO loss functions have a tunable complexity based on the order of the polynomial; third-order functions were identified to work best in practical settings.

The third-order TaylorGLO loss function parameterization provides a fixed representation that can be used to analyze a large family of loss functions through a unified methodology. In prior work, TaylorGLO loss functions were shown to improve generalization empirically [Gonzalez and Miikkulainen 2021]. This paper complements that work, explaining why that is the case by analyzing the dynamics of training theoretically.

Next, the TaylorGLO parameterization and the evolutionary optimization approach that leverages it are discussed in Section 3 and Section 4, respectively.

3 LOSS FUNCTIONS AS MULTIVARIATE TAYLOR EXPANSIONS

Taylor expansions [Taylor 1715] are a well-known function approximator that can represent differentiable functions within the neighborhood of a point using a polynomial series. Below, the common univariate Taylor expansion formulation is presented, followed by a natural extension to arbitrarily-multivariate functions.

Given a $C^{k_{\max}}$ smooth (i.e., first through k_{\max} derivatives are continuous), real-valued function, $f(x) : \mathbb{R} \rightarrow \mathbb{R}$, a k th-order Taylor approximation at point $a \in \mathbb{R}$, $\hat{f}_k(x, a)$, where $0 \leq k \leq k_{\max}$, can be constructed as

$$\hat{f}_k(x, a) = \sum_{n=0}^k \frac{1}{n!} f^{(n)}(a)(x - a)^n. \quad (1)$$

Conventional, univariate Taylor expansions have a natural extension to arbitrarily high-dimensional inputs of f . Given a $C^{k_{\max}+1}$ smooth, real-valued function, $f(\mathbf{x}) : \mathbb{R}^n \rightarrow \mathbb{R}$, a k th-order Taylor approximation at point $\mathbf{a} \in \mathbb{R}^n$, $\hat{f}_k(\mathbf{x}, \mathbf{a})$, where $0 \leq k \leq k_{\max}$, can be constructed. The stricter smoothness constraint compared to the univariate case allows for the application of Schwarz's theorem on equality of mixed partials, obviating the need to take the order of partial differentiation into account.

Let us define an n th-degree multi-index, $\alpha = (\alpha_1, \alpha_2, \dots, \alpha_n)$, where $\alpha_i \in \mathbb{N}_0$, $|\alpha| = \sum_{i=1}^n \alpha_i$, $\alpha! = \prod_{i=1}^n \alpha_i!$, $\mathbf{x}^\alpha = \prod_{i=1}^n x_i^{\alpha_i}$, and $\mathbf{x} \in \mathbb{R}^n$. Multivariate partial derivatives can be concisely written using a multi-index

$$\partial^\alpha f = \partial_1^{\alpha_1} \partial_2^{\alpha_2} \dots \partial_n^{\alpha_n} f = \frac{\partial^{|\alpha|}}{\partial x_1^{\alpha_1} \partial x_2^{\alpha_2} \dots \partial x_n^{\alpha_n}}. \quad (2)$$

Thus, discounting the remainder term, the multivariate Taylor expansion for $f(\mathbf{x})$ at \mathbf{a} is

$$\hat{f}_k(\mathbf{x}, \mathbf{a}) = \sum_{\forall \alpha, |\alpha| \leq k} \frac{1}{\alpha!} \partial^\alpha f(\mathbf{a}) (\mathbf{x} - \mathbf{a})^\alpha. \quad (3)$$

The unique partial derivatives in \hat{f}_k and \mathbf{a} are parameters for a k th order Taylor expansion. Thus, a k th order Taylor expansion of a function in n variables requires n parameters to define the center, \mathbf{a} , and one parameter for each unique multi-index α , where $|\alpha| \leq k$. That is:

$$\#_{\text{parameters}}(n, k) = n + \binom{n+k}{k} = n + \frac{(n+k)!}{n! k!}. \quad (4)$$

The multivariate Taylor expansion can be leveraged for a novel loss-function parameterization [Gonzalez and Miikkulainen 2021]. Let an n -class classification loss function be defined as $\mathcal{L}_{\text{Log}} = -\frac{1}{n} \sum_{i=1}^n f(x_i, y_i)$. The function $f(x_i, y_i)$ can be replaced by its k th-order, bivariate Taylor expansion, $\hat{f}_k(x, y, a_x, a_y)$. More sophisticated loss functions can be supported by having more input variables beyond x_i and y_i , such as a time variable or unscaled logits. This approach can be useful, for example, to evolve loss functions that change as training progresses.

For example, a loss function in \mathbf{x} and \mathbf{y} has the following third-order parameterization with parameters θ (where $\mathbf{a} = \langle \theta_0, \theta_1 \rangle$):

$$\begin{aligned} \mathcal{L}(\mathbf{x}, \mathbf{y}) = & -\frac{1}{n} \sum_{i=1}^n \left[\theta_2 + \theta_3(y_i - \theta_1) + \frac{1}{2}\theta_4(y_i - \theta_1)^2 \right. \\ & + \frac{1}{6}\theta_5(y_i - \theta_1)^3 + \theta_6(x_i - \theta_0) + \theta_7(x_i - \theta_0)(y_i - \theta_1) \\ & + \frac{1}{2}\theta_8(x_i - \theta_0)(y_i - \theta_1)^2 + \frac{1}{2}\theta_9(x_i - \theta_0)^2 \\ & \left. + \frac{1}{2}\theta_{10}(x_i - \theta_0)^2(y_i - \theta_1) + \frac{1}{6}\theta_{11}(x_i - \theta_0)^3 \right] \end{aligned} \quad (5)$$

Notably, the reciprocal-factorial coefficients can be integrated to be a part of the parameter set by direct multiplication if desired.

As was shown by Gonzalez and Miikkulainen [2021], the technique makes it possible to train neural networks that are more accurate and learn faster than those with tree-based loss function representations. Representing loss functions in this manner confers several useful properties:

- It guarantees smooth functions;
- Functions do not have poles (i.e., discontinuities going to infinity or negative infinity) within their relevant domain;
- They can be implemented purely as compositions of addition and multiplication operations;
- They can be trivially differentiated;

- Nearby points in the search space yield similar results (i.e., the search space is locally smooth), making the fitness landscape easier to search;
- Valid loss functions can be found in fewer generations and with higher frequency;
- Loss function discovery is consistent and not dependent on a specific initial population; and
- The search space has a tunable complexity parameter (i.e., the order of the expansion).

These properties are not necessarily held by alternative function approximators. For instance:

Fourier series are well suited for approximating periodic functions [Fourier 1829]. Consequently, they are not as well suited for loss functions, whose local behavior within a narrow domain is important. Being a composition of waves, Fourier series tend to have many critical points within the domain of interest. Gradients fluctuate around such points, making gradient descent infeasible. Additionally, close approximations require a large number of terms, which in itself can be injurious, causing large, high-frequency fluctuations known as “ringing”, due to Gibb’s phenomenon [Wilbraham 1848].

Padé approximants can be more accurate approximations than Taylor expansions; indeed, Taylor expansions are a special case of Padé approximants where $M = 0$ [Graves-Morris 1979]. However, unfortunately Padé approximants can model functions with one or more poles, which valid loss functions typically should not have. These problems still exist, and are exacerbated, for Chisholm approximants (a bivariate extension) [Chisholm 1973]) and Canterbury approximants (a multivariate generalization) [Graves-Morris and Roberts 1975].

Laurent polynomials can represent functions with discontinuities, the simplest being x^{-1} . While Laurent polynomials provide a generalization of Taylor expansions into negative exponents, the extension is not useful because it results in the same issues as Padé approximants.

Polyharmonic splines can represent continuous functions within a finite domain, however, the number of parameters is prohibitive in multivariate cases.

The multivariate Taylor expansion is therefore a better choice than the alternatives. It makes it possible to optimize loss functions efficiently in TaylorGLO, as will be described next.

4 THE TAYLORGLO METHOD

TaylorGLO¹ (Figure 1) aims to find the optimal parameters for a loss function represented as a multivariate Taylor expansion. The parameters for a Taylor approximation (i.e., the center point and partial derivatives) are referred to as $\theta_{\hat{f}}: \theta_{\hat{f}} \in \Theta, \Theta = \mathbb{R}^{\#\text{parameters}}$. TaylorGLO strives to find the vector $\theta_{\hat{f}}^*$ that parameterizes the optimal loss function for a task. Because the values are continuous, as opposed to discrete graphs of the original GLO, it is possible to use continuous optimization methods.

In particular, Covariance Matrix Adaptation Evolutionary Strategy [CMA-ES; Hansen and Ostermeier 1996] is a popular population-based, black-box optimization technique for rugged, continuous spaces. CMA-ES functions by maintaining a covariance matrix around a mean point that represents a distribution of solutions. At each generation, CMA-ES adapts the distribution to better fit evaluated objective values from sampled individuals. In this manner, the area in the search space that is being sampled at each step grows, shrinks, and moves dynamically as needed to maximize sampled candidates’ fitnesses. TaylorGLO uses the $(\mu/\mu, \lambda)$ variant of CMA-ES [Hansen and Ostermeier 2001], which incorporates weighted rank- μ updates [Hansen and Kern 2004] to reduce the number of objective function evaluations needed.

In order to find $\theta_{\hat{f}}^*$, at each generation CMA-ES samples points in Θ . Their fitness is determined by training a model with the corresponding loss function and evaluating the model on a validation

¹Open-source code for TaylorGLO is available at <https://github.com/cognizant-ai-labs/taylorglo>.

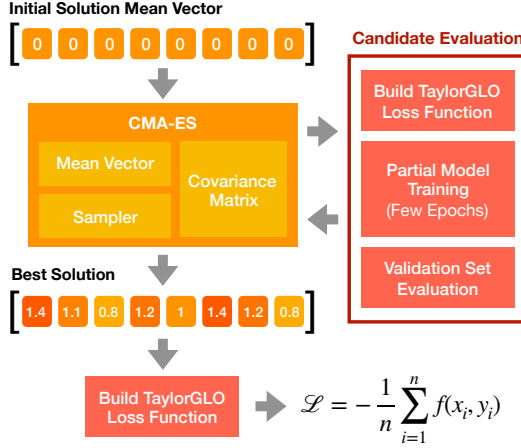


Fig. 1. The TaylorGLO method [Gonzalez and Miikkulainen 2021]. Loss functions are represented by fixed-size vectors whose elements parameterize modified Taylor polynomials. Starting with a population of initially unbiased loss functions (i.e., vectors around the origin), CMA-ES optimizes their Taylor expansion parameters in order to maximize validation accuracy after partial training. The candidate with the highest accuracy is chosen as the final, best solution. This approach biases the search towards functions with useful properties, and is also amenable to theoretical analysis, as shown in this paper.

dataset. Fitness evaluations may be distributed across multiple machines in parallel and retried a limited number of times upon failure. An initial vector of $\theta_{\hat{f}} = \mathbf{0}$ is chosen as a starting point in the search space to avoid bias.

Fully training a model can be prohibitively expensive in many problems. However, performance near the beginning of training is usually correlated with performance at the end of training, and therefore it is enough to train the models only partially to identify the most promising candidates. This type of approximate evaluation is common in metalearning [Grefenstette and Fitzpatrick 1985; Jin 2011]. An additional positive effect is that evaluation then favors loss functions that learn more quickly.

For a loss function to be useful, it must have a derivative that depends on the prediction. Therefore, internal terms that do not contribute to $\frac{\partial}{\partial y} \mathcal{L}_f(\mathbf{x}, \mathbf{y})$ can be trimmed away. This step implies that any term t within $f(x_i, y_i)$ with $\frac{\partial}{\partial y_i} t = 0$ can be replaced with 0. For example, this refinement simplifies Equation 5, providing a reduction in the number of parameters from twelve to eight:

$$\mathcal{L}(\mathbf{x}, \mathbf{y}) = -\frac{1}{n} \sum_{i=1}^n \left[\theta_2(y_i - \theta_1) + \frac{1}{2}\theta_3(y_i - \theta_1)^2 + \frac{1}{6}\theta_4(y_i - \theta_1)^3 \right. \\ \left. + \theta_5(x_i - \theta_0)(y_i - \theta_1) + \frac{1}{2}\theta_6(x_i - \theta_0)(y_i - \theta_1)^2 \right. \\ \left. + \frac{1}{2}\theta_7(x_i - \theta_0)^2(y_i - \theta_1) \right]. \quad (6)$$

Building on this foundation, a theoretical framework for analyzing TaylorGLO will be developed next.

5 LEARNING RULE DECOMPOSITION

The main idea is to decompose the learning rule so that the contribution of the loss function becomes clear. Comparisons of different loss functions can then be drawn at different stages of the training process. For an overview of the notation, see Appendix A.

To begin, consider the standard SGD update rule:

$$\boldsymbol{\theta} \leftarrow \boldsymbol{\theta} - \eta \nabla_{\boldsymbol{\theta}} (\mathcal{L}(\mathbf{x}_i, \mathbf{y}_i, \boldsymbol{\theta})). \quad (7)$$

where η is the learning rate, $\mathcal{L}(\mathbf{x}_i, \mathbf{y}_i, \boldsymbol{\theta})$ is the loss function applied to the network $h(\mathbf{x}_i, \boldsymbol{\theta})$, \mathbf{x}_i is an input data sample, \mathbf{y}_i is the i th sample's corresponding label, and $\boldsymbol{\theta}$ is the set of trainable parameters in the model. The update for a single weight θ_j is

$$\theta_j \leftarrow \theta_j - \eta D_j (\mathcal{L}(\mathbf{x}_i, \mathbf{y}_i, \boldsymbol{\theta})) = \theta_j - \eta \frac{\partial}{\partial s} \mathcal{L}(\mathbf{x}_i, \mathbf{y}_i, \boldsymbol{\theta} + s\mathbf{j}) \Big|_{s \rightarrow 0}. \quad (8)$$

where \mathbf{j} is a basis vector for the j th weight. This general learning rule can then be decomposed in a classification context for a variety of loss functions: mean squared error (MSE), the cross-entropy loss function, the general third-order TaylorGLO loss function, and the Baikal loss function. Each decomposition results in a learning rule of the form

$$\theta_j \leftarrow \theta_j + \eta \frac{1}{n} \sum_{k=1}^n [\gamma_k(\mathbf{x}_i, \mathbf{y}_i, \boldsymbol{\theta}) D_j (h_k(\mathbf{x}_i, \boldsymbol{\theta}))], \quad (9)$$

where $\gamma_k(\mathbf{x}_i, \mathbf{y}_i, \boldsymbol{\theta})$ is an expression that is specific to each loss function.

Substituting the **Mean squared error (MSE)** loss into Equation 8,

$$\theta_j \leftarrow \theta_j - \eta \frac{1}{n} \sum_{k=1}^n \left[2 (h_k(\mathbf{x}_i, \boldsymbol{\theta} + s\mathbf{j}) - y_{ik}) \frac{\partial}{\partial s} h_k(\mathbf{x}_i, \boldsymbol{\theta} + s\mathbf{j}) \right] \Big|_{s \rightarrow 0} \quad (10)$$

$$= \theta_j + \eta \frac{1}{n} \sum_{k=1}^n \left[2 (y_{ik} - h_k(\mathbf{x}_i, \boldsymbol{\theta})) \frac{\partial}{\partial s} h_k(\mathbf{x}_i, \boldsymbol{\theta} + s\mathbf{j}) \right] \Big|_{s \rightarrow 0}, \quad (11)$$

and breaking up the coefficient expressions into $\gamma_k(\mathbf{x}_i, \mathbf{y}_i, \boldsymbol{\theta})$ results in the weight update step

$$\gamma_k(\mathbf{x}_i, \mathbf{y}_i, \boldsymbol{\theta}) = 2y_{ik} - 2h_k(\mathbf{x}_i, \boldsymbol{\theta}). \quad (12)$$

Substituting the **Cross-entropy loss** into Equation 8,

$$\theta_j \leftarrow \theta_j + \eta \frac{1}{n} \sum_{k=1}^n \left[y_{ik} \frac{1}{h_k(\mathbf{x}_i, \boldsymbol{\theta} + s\mathbf{j})} \frac{\partial}{\partial s} h_k(\mathbf{x}_i, \boldsymbol{\theta} + s\mathbf{j}) \right] \Big|_{s \rightarrow 0} \quad (13)$$

$$= \theta_j + \eta \frac{1}{n} \sum_{k=1}^n \left[\frac{y_{ik}}{h_k(\mathbf{x}_i, \boldsymbol{\theta})} \frac{\partial}{\partial s} h_k(\mathbf{x}_i, \boldsymbol{\theta} + s\mathbf{j}) \right] \Big|_{s \rightarrow 0}, \quad (14)$$

and breaking up the coefficient expressions into $\gamma_k(\mathbf{x}_i, \mathbf{y}_i, \boldsymbol{\theta})$ results in the weight update step

$$\gamma_k(\mathbf{x}_i, \mathbf{y}_i, \boldsymbol{\theta}) = \frac{y_{ik}}{h_k(\mathbf{x}_i, \boldsymbol{\theta})}. \quad (15)$$

Substituting the **Baikal loss** into Equation 8,

$$\theta_j \leftarrow \theta_j + \eta \frac{1}{n} \sum_{k=1}^n \left[\left(\frac{1}{h_k(\mathbf{x}_i, \boldsymbol{\theta} + s\mathbf{j})} + \frac{y_{ik}}{h_k(\mathbf{x}_i, \boldsymbol{\theta} + s\mathbf{j})^2} \right) \frac{\partial}{\partial s} h_k(\mathbf{x}_i, \boldsymbol{\theta} + s\mathbf{j}) \right] \Big|_{s \rightarrow 0} \quad (16)$$

$$= \theta_j + \eta \frac{1}{n} \sum_{k=1}^n \left[\left(\frac{1}{h_k(\mathbf{x}_i, \boldsymbol{\theta})} + \frac{y_{ik}}{h_k(\mathbf{x}_i, \boldsymbol{\theta})^2} \right) \frac{\partial}{\partial s} h_k(\mathbf{x}_i, \boldsymbol{\theta} + s\mathbf{j}) \Big|_{s \rightarrow 0} \right], \quad (17)$$

and breaking up the coefficient expressions into $\gamma_k(\mathbf{x}_i, \mathbf{y}_i, \boldsymbol{\theta})$ results in the weight update step

$$\gamma_k(\mathbf{x}_i, \mathbf{y}_i, \boldsymbol{\theta}) = \frac{1}{h_k(\mathbf{x}_i, \boldsymbol{\theta})} + \frac{y_{ik}}{h_k(\mathbf{x}_i, \boldsymbol{\theta})^2}. \quad (18)$$

Substituting the **Third-order TaylorGLO loss** with parameters λ into Equation 8,

$$\begin{aligned} \theta_j \leftarrow \theta_j + \eta \frac{1}{n} \sum_{k=1}^n \left[\lambda_2 \frac{\partial}{\partial s} h_k(\mathbf{x}_i, \boldsymbol{\theta} + s\mathbf{j}) + \lambda_3 2 (h_k(\mathbf{x}_i, \boldsymbol{\theta} + s\mathbf{j}) - \lambda_1) \frac{\partial}{\partial s} h_k(\mathbf{x}_i, \boldsymbol{\theta} + s\mathbf{j}) \right. \\ \left. + \lambda_4 3 (h_k(\mathbf{x}_i, \boldsymbol{\theta} + s\mathbf{j}) - \lambda_1)^2 \frac{\partial}{\partial s} h_k(\mathbf{x}_i, \boldsymbol{\theta} + s\mathbf{j}) + \lambda_5 (y_{ik} - \lambda_0) \frac{\partial}{\partial s} h_k(\mathbf{x}_i, \boldsymbol{\theta} + s\mathbf{j}) \right. \\ \left. + (\lambda_6 (y_{ik} - \lambda_0) 2 (h_k(\mathbf{x}_i, \boldsymbol{\theta} + s\mathbf{j}) - \lambda_1) + \lambda_7 (y_{ik} - \lambda_0)^2) \frac{\partial}{\partial s} h_k(\mathbf{x}_i, \boldsymbol{\theta} + s\mathbf{j}) \right] \Big|_{s \rightarrow 0} \end{aligned} \quad (19)$$

$$\begin{aligned} = \theta_j + \eta \frac{1}{n} \sum_{k=1}^n \left[(\lambda_3 + \lambda_6 (y_{ik} - \lambda_0)) 2 (h_k(\mathbf{x}_i, \boldsymbol{\theta} + s\mathbf{j}) - \lambda_1) \frac{\partial}{\partial s} h_k(\mathbf{x}_i, \boldsymbol{\theta} + s\mathbf{j}) \Big|_{s \rightarrow 0} \right. \\ \left. + (\lambda_2 + \lambda_5 (y_{ik} - \lambda_0) + \lambda_7 (y_{ik} - \lambda_0)^2) \frac{\partial}{\partial s} h_k(\mathbf{x}_i, \boldsymbol{\theta} + s\mathbf{j}) \Big|_{s \rightarrow 0} \right. \\ \left. + \lambda_4 3 (h_k(\mathbf{x}_i, \boldsymbol{\theta}) - \lambda_1)^2 \frac{\partial}{\partial s} h_k(\mathbf{x}_i, \boldsymbol{\theta} + s\mathbf{j}) \Big|_{s \rightarrow 0} \right], \end{aligned} \quad (20)$$

and breaking up the coefficient expressions into $\gamma_k(\mathbf{x}_i, \mathbf{y}_i, \boldsymbol{\theta})$ results in the weight update step

$$\begin{aligned} \gamma_k(\mathbf{x}_i, \mathbf{y}_i, \boldsymbol{\theta}) = (\lambda_3 + \lambda_6 (y_{ik} - \lambda_0)) 2 (h_k(\mathbf{x}_i, \boldsymbol{\theta}) - \lambda_1) \\ + \lambda_2 + \lambda_5 (y_{ik} - \lambda_0) + \lambda_7 (y_{ik} - \lambda_0)^2 + \lambda_4 3 (h_k(\mathbf{x}_i, \boldsymbol{\theta}) - \lambda_1)^2 \end{aligned} \quad (21)$$

$$\begin{aligned} = 2\lambda_3 h_k(\mathbf{x}_i, \boldsymbol{\theta}) - 2\lambda_1 \lambda_3 + 2\lambda_6 h_k(\mathbf{x}_i, \boldsymbol{\theta}) y_{ik} - 2\lambda_6 \lambda_0 h_k(\mathbf{x}_i, \boldsymbol{\theta}) \\ - 2\lambda_1 \lambda_6 y_{ik} + 2\lambda_1 \lambda_6 \lambda_0 + \lambda_2 + \lambda_5 y_{ik} - \lambda_5 \lambda_0 + \lambda_7 y_{ik}^2 - 2\lambda_7 \lambda_0 y_{ik} \\ + \lambda_7 \lambda_0^2 + 3\lambda_4 h_k(\mathbf{x}_i, \boldsymbol{\theta})^2 - 6\lambda_1 \lambda_4 h_k(\mathbf{x}_i, \boldsymbol{\theta}) + 3\lambda_4 \lambda_1^2. \end{aligned} \quad (22)$$

To simplify analysis in this case, $\gamma_k(\mathbf{x}_i, \mathbf{y}_i, \boldsymbol{\theta})$ can be decomposed into a linear combination of

$$[1, h_k(\mathbf{x}_i, \boldsymbol{\theta}), h_k(\mathbf{x}_i, \boldsymbol{\theta})^2, h_k(\mathbf{x}_i, \boldsymbol{\theta}) y_{ik}, y_{ik}, y_{ik}^2] \quad (23)$$

with respective coefficients $[c_1, c_h, c_{hh}, c_{hy}, c_y, c_{yy}]$ whose values are implicitly functions of λ :

$$\gamma_k(\mathbf{x}_i, \mathbf{y}_i, \boldsymbol{\theta}) = c_1 + c_h h_k(\mathbf{x}_i, \boldsymbol{\theta}) + c_{hh} h_k(\mathbf{x}_i, \boldsymbol{\theta})^2 + c_{hy} h_k(\mathbf{x}_i, \boldsymbol{\theta}) y_{ik} + c_y y_{ik} + c_{yy} y_{ik}^2. \quad (24)$$

Using these decompositions, it is possible to characterize and compare training dynamics different loss functions, as will be done in the next section.

6 CHARACTERIZING TRAINING DYNAMICS

The decompositions are first analyzed at the null epoch, i.e. the initial state of the learning process, when network weights are similarly distributed. This analysis leads to a learning invariant that can be used to make evolution more effective, as will be discussed in Section 7. Behavior at the opposite end of the training process will then be analyzed, i.e. in the zero training error regime. In this regime it is possible to identify optimization biases that lead to implicit regularization. Third, generalizing to the entire training process, a theoretical constraint is derived on the entropy of a network's outputs. This constraint makes it possible to characterize learning in TaylorGLO as an interaction

between data fitting and regularization. Fourth, a secondary mechanism for regularization, implicit label smoothing, is identified. TaylorGLO may discover and utilize label smoothing as part of effective loss functions.

6.1 Behavior at the null epoch

Consider the first epoch of training. Assume all weights are randomly initialized:

$$\forall k \in [1, n], \text{ where } n \geq 2 : \mathbb{E}_i [h_k(\mathbf{x}_i, \boldsymbol{\theta})] = \frac{1}{n}. \quad (25)$$

That is, logits are distributed with high entropy. Behavior at the null epoch can then be defined piecewise for target vs. non-target logits for each loss function.

In the case of **Mean squared error (MSE)**,

$$\gamma_k(\mathbf{x}_i, \mathbf{y}_i, \boldsymbol{\theta}) = \begin{cases} 2n^{-1} & y_{ik} = 0 \\ 2n^{-1} - 2 & y_{ik} = 1. \end{cases} \quad (26)$$

Since $n \geq 2$, the $y_{ik} = 1$ case will always be negative, while the $y_{ik} = 0$ case will always be positive. Thus, target scaled logits will be maximized and non-target scaled logits minimized.

In the case of **Cross-entropy loss**,

$$\gamma_k(\mathbf{x}_i, \mathbf{y}_i, \boldsymbol{\theta}) = \begin{cases} 0 & y_{ik} = 0 \\ n & y_{ik} = 1. \end{cases} \quad (27)$$

Target scaled logits are maximized and, consequently, non-target scaled logits minimized as a result of the softmax function.

Similarly in the case of **Baikal loss**,

$$\gamma_k(\mathbf{x}_i, \mathbf{y}_i, \boldsymbol{\theta}) = \begin{cases} n & y_{ik} = 0 \\ n + n^2 & y_{ik} = 1. \end{cases} \quad (28)$$

Target scaled logits are minimized and, consequently, non-target scaled logits minimized as a result of the softmax function (since the $y_{ik} = 1$ case dominates).

In the case of **Third-order TaylorGLO loss**, since behavior is highly dependent on $\boldsymbol{\lambda}$, consider the concrete loss function that TaylorGLO discovered for the ALLCNN-C model on CIFAR-10 [Gonzalez and Miikkulainen 2021]:

$$\gamma_k(\mathbf{x}_i, \mathbf{y}_i, \boldsymbol{\theta}) = \begin{cases} -373.917 - 130.264 h_k(\mathbf{x}_i, \boldsymbol{\theta}) - 11.2188 h_k(\mathbf{x}_i, \boldsymbol{\theta})^2 & y_{ik} = 0 \\ -372.470735 - 131.47 h_k(\mathbf{x}_i, \boldsymbol{\theta}) - 11.2188 h_k(\mathbf{x}_i, \boldsymbol{\theta})^2 & y_{ik} = 1. \end{cases} \quad (29)$$

Note that Equation 38 is a special case of this behavior where $h_k(\mathbf{x}_i, \boldsymbol{\theta}) = y_{ik}$. Let us substitute $h_k(\mathbf{x}_i, \boldsymbol{\theta}) = \frac{1}{n}$ (i.e., the expected value of a logit at the null epoch):

$$\gamma_k(\mathbf{x}_i, \mathbf{y}_i, \boldsymbol{\theta}) = \begin{cases} -373.917 - 130.264 n^{-1} - 11.2188 n^{-2} & y_{ik} = 0 \\ -372.470735 - 131.47 n^{-1} - 11.2188 n^{-2} & y_{ik} = 1. \end{cases} \quad (30)$$

Since this loss function was found on CIFAR-10, a 10-class image classification task, $n = 10$:

$$\gamma_k(\mathbf{x}_i, \mathbf{y}_i, \boldsymbol{\theta}) = \begin{cases} -386.9546188 & y_{ik} = 0 \\ -385.729923 & y_{ik} = 1. \end{cases} \quad (31)$$

Since both cases of $\gamma_k(\mathbf{x}_i, \mathbf{y}_i, \boldsymbol{\theta})$ are negative, this behavior implies that all scaled logits will be minimized. However, since the scaled logits are the output of a softmax function, and the $y_{ik} = 0$

case is more strongly negative, the non-target scaled logits will be minimized more than the target scaled logits, resulting in a maximization of the target scaled logits.

The desired behavior at the null epoch is clear, and the above evaluated loss functions all exhibit it. However, certain settings for λ in TaylorGLO loss functions may result in detrimental behavior. Thus, a constraint on λ can be derived to make sure that it does not happen. Such a constraint is derived in Appendix E and used to speed up the TaylorGLO search process in Section 7.

Next, the opposite end of the training process is analyzed in order to identify optimization biases with different loss functions. They will lead to understanding of the regularization mechanisms in TaylorGLO, as will be discussed in Section 6.3.

6.2 Optimization biases in the zero training error regime

Certain biases in optimization imposed by a loss function can be best observed in the case where there is nothing new to learn from the training data. Consider the case where there is zero training error, that is, $h_k(\mathbf{x}_i, \boldsymbol{\theta}) - y_{ik} = 0$. In this case, all $h_k(\mathbf{x}_i, \boldsymbol{\theta})$ can be substituted with y_{ik} in $\gamma_k(\mathbf{x}_i, \mathbf{y}_i, \boldsymbol{\theta})$, as is done below for the different loss functions.

Mean squared error (MSE): In this case,

$$\gamma_k(\mathbf{x}_i, \mathbf{y}_i, \boldsymbol{\theta}) = 2y_{ik} - 2h_k(\mathbf{x}_i, \boldsymbol{\theta}) = 0. \quad (32)$$

Thus, there are no changes to the weights of the model once error reaches zero. This observation contrasts with the findings in Blanc et al. [2020], who discovered an implicit regularization effect when training with MSE loss *and* label noise. Notably, this null behavior is representable in a non-degenerate TaylorGLO parameterization, since MSE is itself representable by TaylorGLO with $\lambda = [0, 0, 0, -1, 0, 2, 0, 0]$. Thus, this behavior can be leveraged in evolved loss functions.

Cross-entropy loss: Since $h_k(\mathbf{x}_i, \boldsymbol{\theta}) = 0$ for non-target logits in a zero training error regime, $\gamma_k(\mathbf{x}_i, \mathbf{y}_i, \boldsymbol{\theta}) = \frac{0}{0}$, i.e. an indeterminate form. Thus, an arbitrarily-close-to-zero training error regime is analyzed instead, such that $h_k(\mathbf{x}_i, \boldsymbol{\theta}) = \epsilon$ for non-target logits for an arbitrarily small ϵ . Since all scaled logits sum to 1, $h_k(\mathbf{x}_i, \boldsymbol{\theta}) = 1 - (n - 1)\epsilon$ for the target logit. Let us analyze the learning rule as ϵ tends towards 0:

$$\theta_j \leftarrow \theta_j + \lim_{\epsilon \rightarrow 0} \eta \frac{1}{n} \sum_{k=1}^n \begin{cases} \frac{y_{ik}}{\epsilon} D_j(h_k(\mathbf{x}_i, \boldsymbol{\theta})) & y_{ik} = 0 \\ \frac{y_{ik}}{1 - (n - 1)\epsilon} D_j(h_k(\mathbf{x}_i, \boldsymbol{\theta})) & y_{ik} = 1 \end{cases} \quad (33)$$

$$= \theta_j + \eta \frac{1}{n} \sum_{k=1}^n \begin{cases} 0 & y_{ik} = 0 \\ D_j(h_k(\mathbf{x}_i, \boldsymbol{\theta})) & y_{ik} = 1. \end{cases} \quad (34)$$

Intuitively, this learning rule aims to increase the value of the target scaled logits. Since logits are scaled by a softmax function, increasing the value of one logit decreases the values of other logits. Thus, the fixed point of this bias will be to force non-target scaled logits to zero, and target scaled logits to one. In other words, this behavior aims to minimize the divergence between the predicted distribution and the training data's distribution.

TaylorGLO can represent this behavior, and can thus be leveraged in evolved loss functions, through any case where $a = 0$ and $b + c > 0$. Any λ where $\lambda_2 = 2\lambda_1\lambda_3 + \lambda_5\lambda_0 - 2\lambda_1\lambda_6\lambda_0 - \lambda_7\lambda_0^2 - 3\lambda_4\lambda_1^2$ represents such a satisfying family of cases. Additionally, TaylorGLO allows for the strength of this bias to be tuned independently from η by adjusting the magnitude of $b + c$.

Baikal loss: The Baikal loss function results in infinite gradients at zero training error, rendering

it unstable, even if using it to fine-tune from a previously trained network that already reached zero training error. However, the zero-error regime is irrelevant with Baikal because it cannot be reached in practice:

Theorem 1: Zero training error regions of the weight space are not attractors for the Baikal loss function.

The reason is that if a network reaches a training error that is arbitrarily close to zero, there is a repulsive effect that biases the model’s weights away from zero training error. Proof of this theorem is in Appendix B.

Third-order TaylorGLO loss:² According to Equation 24, in the zero-error regime, $\gamma_k(\mathbf{x}_i, \mathbf{y}_i, \boldsymbol{\theta})$ can be written as a linear combination $\gamma_k(\mathbf{x}_i, \mathbf{y}_i, \boldsymbol{\theta}) = a + by_{ik} + cy_{ik}^2$, where

$$a = \lambda_2 - 2\lambda_1\lambda_3 - \lambda_5\lambda_0 + 2\lambda_1\lambda_6\lambda_0 + \lambda_7\lambda_0^2 + 3\lambda_4\lambda_1^2 \quad (35)$$

$$b = 2\lambda_3 - 2\lambda_6\lambda_0 - 2\lambda_1\lambda_6 + \lambda_5 - 2\lambda_7\lambda_0 - 6\lambda_4\lambda_1 \quad (36)$$

$$c = 2\lambda_6 + \lambda_7 + 3\lambda_4. \quad (37)$$

The learning rule thus becomes

$$\theta_j \leftarrow \theta_j + \eta \frac{1}{n} \sum_{k=1}^n \begin{cases} aD_j(h_k(\mathbf{x}_i, \boldsymbol{\theta})) & y_{ik} = 0 \\ (a + b + c)D_j(h_k(\mathbf{x}_i, \boldsymbol{\theta})) & y_{ik} = 1. \end{cases} \quad (38)$$

As a concrete example, consider again the TaylorGLO loss function for AllCNN-C on CIFAR-10. It had $a = -373.917$, $b = -129.928$, $c = -11.3145$. Notably, all three coefficients are negative, i.e. all changes to θ_j are a negatively scaled values of $D_j(h_k(\mathbf{x}_i, \boldsymbol{\theta}))$, as can be seen from Equation 38. Thus, there are two competing processes in this learning rule: one that aims to minimize all non-target scaled logits (increasing the scaled logit distribution’s entropy), and one that aims to minimize the target scaled logit (decreasing the scaled logit distribution’s entropy). The processes conflict with each other since logits are scaled through a softmax function. These processes can shift weights in a particular way while maintaining zero training error, which results in implicit regularization. If, however, such shifts in this zero training error regime do lead to misclassifications on the training data, $h_k(\mathbf{x}_i, \boldsymbol{\theta})$ would no longer equal y_{ik} , and a non-zero error regime’s learning rule would come into effect. It would strive to get back to zero training error with a different $\boldsymbol{\theta}$.

Similarly to Baikal loss, a training error of exactly zero is not an attractor for some third-order TaylorGLO loss functions (this property can be seen through an analysis similar to that in Appendix B). The zero-error case would occur in practice only if this loss function were to be used to fine tune a network that truly has a zero training error. It is, however, a useful step in characterizing the regularization in TaylorGLO, as will be seen in the next section.

6.3 Data fitting vs. regularization throughout learning

In order to characterize regularization throughout the training process, we need to understand how specific training samples affect a network’s trainable parameters. Under what gradient conditions does a network’s softmax function transition from increasing the entropy in the output distribution (i.e. fitting to the data) to decreasing it (i.e. regularization)? Let us analyze the case where all non-target logits have the same value, $\frac{\epsilon}{n-1}$, and the target logit has the value $1 - \epsilon$. That is, all non-target classes have equal probabilities.

²Note that in the basic classification case, $\forall \mathbf{w} \in \mathbb{N}_1 : y_{ik} = y_{ik}^{\mathbf{w}}$, since $y_{ik} \in \{0, 1\}$; This observation provides an intuition for why higher-order TaylorGLO loss functions do not provide fundamentally different behavior, beyond a more overparameterized search space, and thus no improvements in performance, over third-order loss functions.

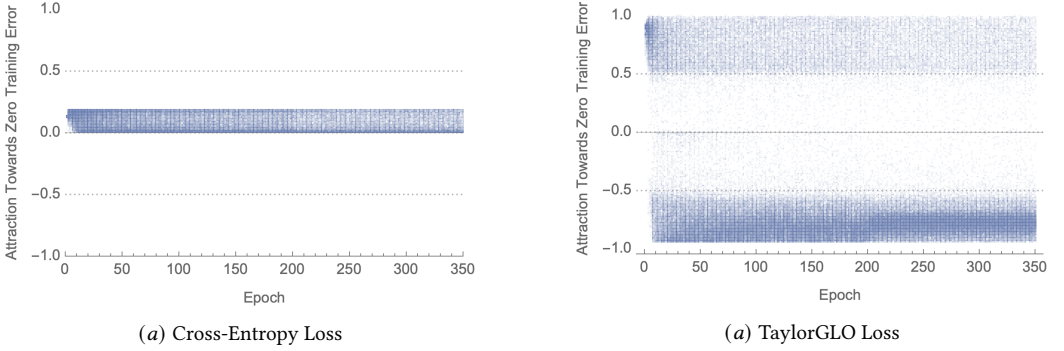


Fig. 2. Per-sample attraction towards zero training error with cross-entropy vs. TaylorGLO loss functions on CIFAR-10 AllCNN-C models. Each point represents an individual training sample (500 are randomly sampled per epoch); its x -location indicates the training epoch, and y -location the strength with which the loss functions pulls the output towards the correct label, or pushes it away from it. With the cross-entropy loss, these values are always positive, indicating a constant pull towards the correct label for every single training sample. Interestingly, the TaylorGLO values span both the positives and the negatives; at the beginning of training there is a strong pull towards the correct label (seen as the dark area on top left), which then changes to more prominent push away from it in later epochs. This plot shows how TaylorGLO regularizes by preventing overconfidence and biasing solutions towards different parts of the weight space.

Theorem 2. The strength of entropy reduction is proportional to

$$\frac{\epsilon(\epsilon - 1) \left(e^{\epsilon(\epsilon-1)(\gamma_{-T}-\gamma_T)} - e^{\frac{\epsilon(\epsilon-1)\gamma_T(n-1)+\epsilon\gamma_{-T}(\epsilon(n-3)+n-1)}{(n-1)^2}} \right)}{(\epsilon - 1) e^{\epsilon(\epsilon-1)(\gamma_{-T}-\gamma_T)} - \epsilon e^{\frac{\epsilon(\epsilon-1)\gamma_T(n-1)+\epsilon\gamma_{-T}(\epsilon(n-3)+n-1)}{(n-1)^2}}} \quad (39)$$

where γ_{-T} is the value of γ_j for non-target logits, and γ_T for the target logit.

Thus, values less than zero imply that entropy is increased, values greater than zero imply that it is decreased, and values equal to zero imply that there is no change. The proof of this theorem is in Appendix C.

The size of reduction in entropy in Theorem 2 can also be thought of as a measure of the strength of the attraction towards zero training error regions of the parameter space (i.e., shrinking non-target logits and growing target logits imply reduced training error). This strength can be calculated for individual training samples during any part of the training process, leading to the insight that the process results from competing “push” and “pull” forces. This theoretical insight, combined with empirical data from actual training sessions, explains how different loss functions balance data fitting and regularization.

Figure 2 provides one such example on AllCNN-C models [Springenberg et al. 2015] trained on CIFAR-10 [Krizhevsky and Hinton 2009] with cross-entropy vs. custom TaylorGLO loss functions. Scaled target and non-target logit values were logged for every sample at every epoch and used to calculate respective γ_T and γ_{-T} values. These values were then substituted into Equation 39 to get the strength of bias towards zero training error.

The cross-entropy loss exhibits a tendency towards zero training error for every single sample, as expected. The TaylorGLO loss, however, has a much different behavior: initially, there is a much stronger pull towards zero training error for all samples—which leads to better generalization [Li et al. 2019; Yao et al. 2007]—after which a stratification occurs, where the majority of samples are

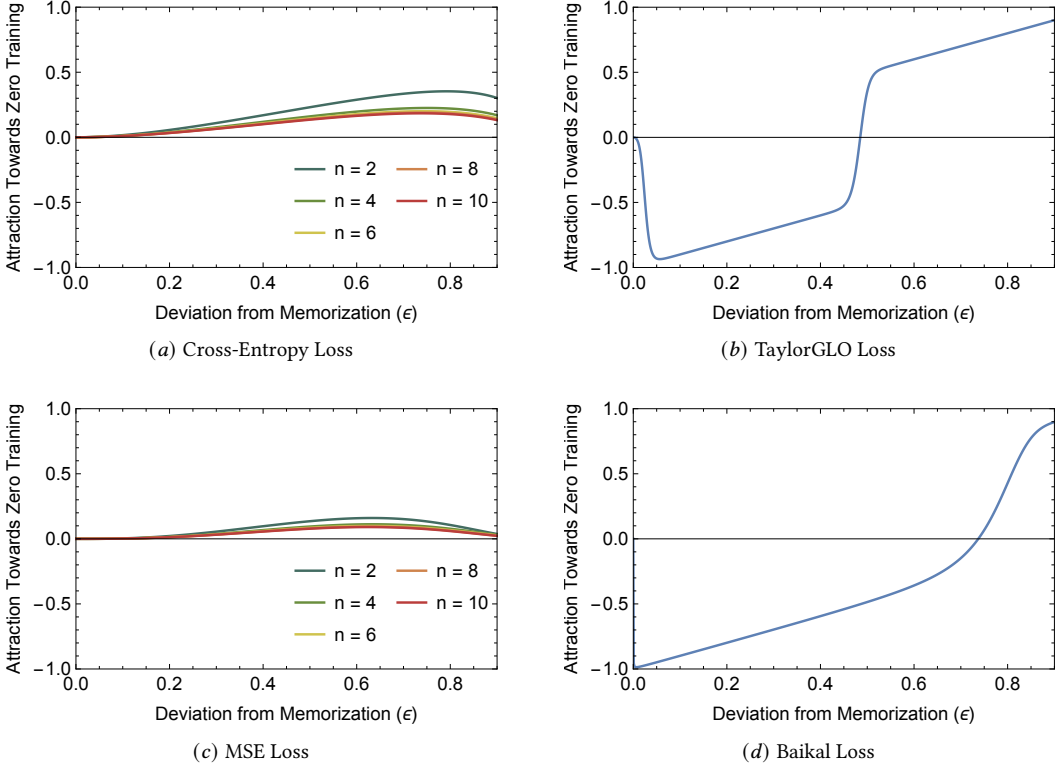


Fig. 3. Attraction towards zero training error with different loss functions. Each loss function has a characteristic curve—plotted using Equation 39—that describes zero training error attraction dynamics for individual samples given their current deviation from perfect memorization, ϵ . Plots (a) and (b) only have the $n = 10$ case plotted, i.e. the 10-class classification case for which they were evolved. Cross-entropy (a) and MSE (c) loss functions have positive attraction for all values of ϵ . In contrast, the TaylorGLO loss function for CIFAR-10 on AII CNN-C (b) and the Baikal loss function (d) both have very strong attraction for weakly learned samples (on the right side), and repulsion for highly confidently learned samples (on the left side). Thus, this illustration provides a graphical intuition for the regularization that TaylorGLO and Baikal loss functions establish.

repelled, and thus biased towards a different region of the weight space with better performance characteristics.

The strength of the attraction towards zero training error regions of the parameter space (described in Theorem 2) can be plotted—for any given number of classes n —at different ϵ values using the corresponding γ_T and γ_{-T} values from a particular loss function. These characteristic curves for four specific loss functions are shown in Figure 3.

Both Baikal and TaylorGLO loss functions have significantly different attraction curves than the cross-entropy and mean squared error loss functions. Cross-entropy and mean squared error always exhibit positive attraction to zero training error. Conversely, TaylorGLO and Baikal exhibit this positive attraction behavior only for samples that are weakly memorized; well memorized samples produce a repulsive effect instead. This difference is what contributes to both metalearned loss functions’ regularizing effects, where overconfidence is avoided.

6.4 Regularization through implicit label smoothing

In the previous section, TaylorGLO loss functions were shown to provide regularization through dynamic biases that are imparted throughout the training process. However, this behavior is not the only way that TaylorGLO can regularize. This section shows how the regularization imparted by label smoothing [Szegedy et al. 2016] can be implicitly represented by TaylorGLO.

Consider a basic setup with standard label smoothing, controlled by a hyperparameter $\alpha \in (0, 1)$, such that the target value in any \mathbf{y}_i is $1 - \alpha \frac{n-1}{n}$ rather than 1, and non-target values are $\frac{\alpha}{n}$ rather than 0.

Theorem 3. For any λ and any $\alpha \in (0, 1)$, there exists a $\hat{\lambda}$ such that the behavior imposed by $\hat{\lambda}$ without explicit label smoothing is identical to the behavior imposed by λ with explicit label smoothing.

That is, any degree of label smoothing can be implicitly represented for any TaylorGLO loss function. Thus, TaylorGLO may discover and utilize label smoothing as part of discovering loss functions, increasing their ability to regularize further. The proof of this theorem is in Appendix D.

Even though the main goal of the theoretical analysis was to understand the regularization mechanisms in loss-function metalearning, it also leads to a surprising insight that allows improving the search in practice, as will be discussed next.

7 INVARIANT ON TAYLORGLO PARAMETERS

As mentioned in Section 6.1, there are many different instances of λ for which models are untrainable. One such case, albeit a degenerate one, is $\lambda = \mathbf{0}$ (i.e., a function with zero gradients everywhere). Given the training dynamics at the null epoch (characterized in Appendix 6.1), more general constraints on λ can be derived, resulting in the following theorem:

Theorem 4. A third-order TaylorGLO loss function is not trainable if the following constraints on λ are satisfied:

$$c_1 + c_y + c_{yy} + \frac{c_h + c_{hy}}{n} + \frac{c_{hh}}{n^2} < (n-1) \left(c_1 + \frac{c_h}{n} + \frac{c_{hh}}{n^2} \right) \quad (40)$$

$$c_y + c_{yy} + \frac{c_{hy}}{n} < (n-2) \left(c_1 + \frac{c_h}{n} + \frac{c_{hh}}{n^2} \right). \quad (41)$$

The proof of this theorem is in Appendix E. These constraints are useful because their inverse can be used as an invariant during loss function evolution. That is, they can be used to identify entire families of loss function parameters that do not result in a viable loss function, rule them out during search, and thereby make the search more effective. More specifically, before each candidate λ is evaluated, it is checked for conformance to the invariant. If the invariant is violated, the algorithm can skip that candidate’s validation training and simply assign a fitness of zero. However, due to the added complexity that the invariant imposes on the fitness landscape, a larger population size is needed for evolution within TaylorGLO to be more stable. Practically, a doubling of the population size from 20 to 40 works well.

Table 1 presents results from TaylorGLO runs with and without the invariant on the CIFAR-10 image classification benchmark dataset [Krizhevsky and Hinton 2009] with various architectures. Networks with Cutout [DeVries and Taylor 2017] were also evaluated to show that TaylorGLO provides a different approach to regularization. Standard training hyperparameters from the references were used for each architecture. Notably, the invariant allows TaylorGLO to discover loss functions

Table 1. Test-set accuracy of loss functions discovered by TaylorGLO with and without an invariant constraint on λ . Models were trained on the loss function that had the highest validation accuracy during the TaylorGLO evolution. All averages are from ten separately trained models and p -values are from one-tailed Welch’s t -Tests. Standard deviations are shown in parentheses. The invariant allows focusing metalearning to viable areas of the search space, resulting in better loss functions.

Task and Model	Avg. TaylorGLO Acc.	+ Invariant	p -value
CIFAR-10 on AlexNet ¹	0.7901 (0.0026)	0.7933 (0.0026)	0.0092
CIFAR-10 on PreResNet-20 ²	0.9169 (0.0014)	0.9164 (0.0019)	0.2827
CIFAR-10 on AllCNN-C ³	0.9271 (0.0013)	0.9290 (0.0014)	0.0004
CIFAR-10 on AllCNN-C ³ + Cutout ⁴	0.9329 (0.0022)	0.9350 (0.0014)	0.0124

¹ Krizhevsky et al. [2012] ² He et al. [2016] ³ Springenberg et al. [2015] ⁴ DeVries and Taylor [2017]

that have statistically significantly better performance in many cases and never a detrimental effect. These results demonstrate that the theoretical invariant is useful in practice, and should become a standard in TaylorGLO applications.

8 ADVERSARIAL ROBUSTNESS

TaylorGLO loss functions discourage overconfidence, i.e. their activations are less extreme and vary more smoothly with input. Such encodings are likely to be more robust against noise, damage, and other imperfections in the data and in the network execution. In the extreme case, they may also be more robust against adversarial attacks. This hypothesis will be tested experimentally in this section, and an empirical explanation will be given in terms of the flatness of loss-surface minima.

8.1 Evaluation with adversarial attacks

Adversarial attacks elicit incorrect predictions from a trained model by changing input samples in small ways that can even be imperceptible. They are generally classified as “white-box” or “black-box” attacks, depending on whether the attacker has access to the underlying model or not, respectively. Naturally, white-box attacks are more powerful at overwhelming a model. One such white-box attack is the Fixed Gradient Sign Method [FGSM; Goodfellow et al. 2015]: following evaluation of a dataset, input gradients are taken from the network following a backward pass. Each individual gradient has its sign calculated and scaled by an ϵ scaling factor that determines the attack strength. These values are added to future network inputs with an ϵ scaling factor, causing misclassifications.

Figure 4 shows how robust networks with different loss functions are against FGSM attacks of various strengths. In the first experiment, AllCNN-C and Wide ResNet 28-5 [Zagoruyko and Komodakis 2016] networks were trained on CIFAR-10 with TaylorGLO and cross-entropy loss; indeed TaylorGLO outperforms the cross-entropy loss models significantly at all attack strengths. Note that in this case, loss functions were evolved simply to perform well, and adversarial robustness emerged as a side benefit.

However, it is also possible to take adversarial attacks into account as an explicit objective in loss function evolution. Since TaylorGLO uses non-differentiable metrics as objectives in its search process, the traditional validation accuracy objective can be replaced with validation accuracy at a particular FGSM attack strength. This approach was taken in the second experiment, also shown in Figure 4. Remarkably, loss functions found in this manner outperform both the previous TaylorGLO loss functions and the cross-entropy loss.

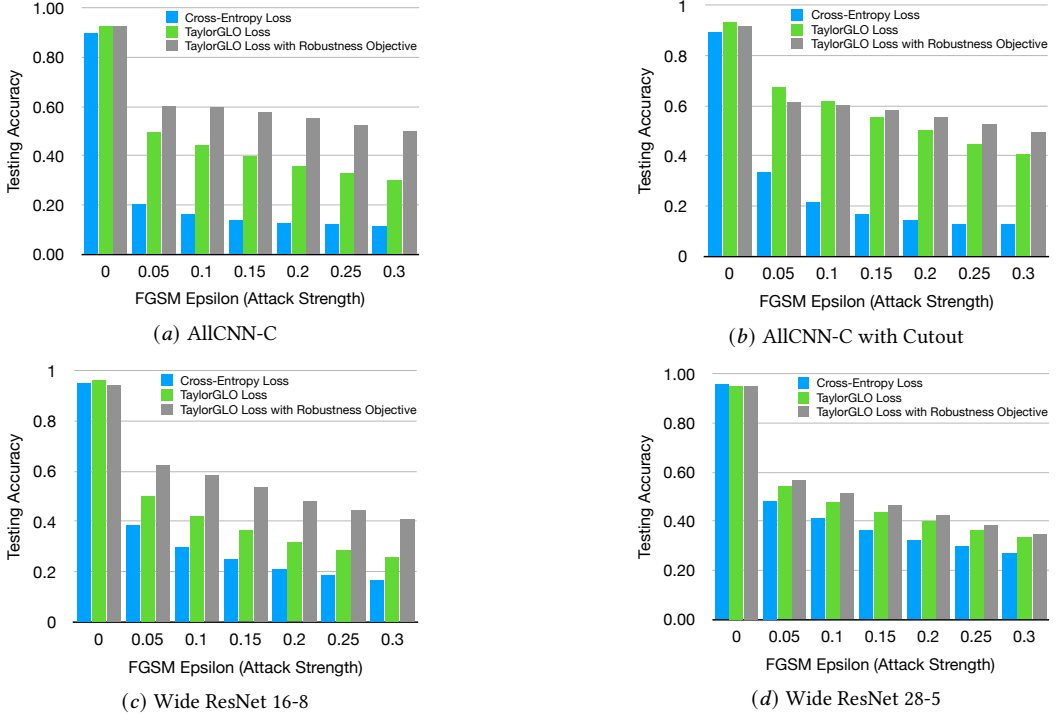


Fig. 4. Robustness of TaylorGLO loss functions against FGSM adversarial attacks with various architectures on CIFAR-10. For each architecture, the blue bars represent accuracy achieved through training with the cross-entropy loss, green bars with a TaylorGLO loss, and gray bars with a TaylorGLO loss specifically evolved in the adversarial attack environment. The leftmost points on each plot represent evaluations without adversarial attacks. TaylorGLO regularization makes the networks more robust against adversarial attacks, and this property can be further enhanced by making it an explicit goal in evolution.

Thus, these results suggest that TaylorGLO regularization leads to robust encoding, and such robustness can be further improved by making it an explicit goal in loss-function optimization. Where the robustness is coming from will be demonstrated next.

8.2 Foundation of robustness

TaylorGLO loss functions are known to result in trained networks with flatter, lower minima [Gonzalez and Miikkulainen 2021]. This result suggests that models trained with TaylorGLO loss function are more robust, i.e. their performance is less sensitive to small perturbations in the weight space, and that they also generalize better [Keskar et al. 2017]. Since TaylorGLO loss functions that were discovered against an adversarial performance objective were even more robust, what do their minima look like?

Model performance can be plotted along a random slice $[-1, 1]$ of the weight space using the loss surface visualization technique of Li et al. [2018]. The random slice vector is normalized in a filter-wise manner to accommodate network weights’ scale invariance, thus ensuring that visualizations for two separate models can be compared. As a result of the randomness, this parameter space slice is unbiased and should take all parameters into account, to a degree. It can therefore be used to perturb trainable parameters systematically.

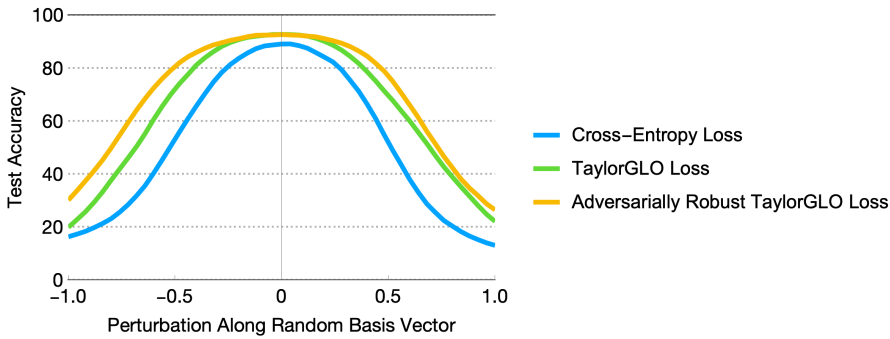


Fig. 5. Comparing accuracy basins of AllCNN-C with cross-entropy, TaylorGLO, and adversarially robust TaylorGLO loss functions on CIFAR-10. Basins are plotted along only one perturbation direction for clarity, using the loss surface visualization technique of Li et al. [2018]. While the adversarially robust TaylorGLO loss function leads to the same accuracy as the standard one, it has a wider, flatter minima. This result suggests that the TaylorGLO loss function that has been evolved to be robust against adversarial attacks is more robust in general, even when adversarial attacks are of no concern.

When AllCNN-C is trained with an adversarially robust versus a standard TaylorGLO loss function, its absolute accuracy is the same. However, the minimum is wider and flatter (Figure 5). This result suggests that it may be advantageous to evaluate TaylorGLO against an adversarial performance metric, even when the target application does not include adversarial attacks.

Future work can naturally extend these analyses to black-box adversarial attacks and adversarial training. Moreover, just as custom loss functions can improve intrinsic robustness against adversarial attacks, custom loss function may make adversarial training more effective.

9 CONCLUSION

Regularization has long been a crucial aspect of training deep neural networks. This paper contributed a theoretical and empirical understanding of one recent and compelling family of regularization techniques: loss-function metalearning. A theoretical framework for representing different loss functions was first developed in order to analyze their training dynamics in various contexts. The results demonstrated that TaylorGLO loss functions implement a guard against overfitting, resulting in automatic regularization. Two practical opportunities emerged from this analysis: filtering based on an invariant was shown to improve the search process, and the robustness against overfitting to make the networks more robust against adversarial attacks. The results thus extend the scope of metalearning, focusing it not just on finding optimal model configurations, but also on improving regularization, learning efficiency, and robustness directly.

REFERENCES

- Antreas Antoniou and Amos J Storkey. 2019. Learning to Learn By Self-Critique. In *Advances in Neural Information Processing Systems*, H. Wallach, H. Larochelle, A. Beygelzimer, F. d'Alché-Buc, E. Fox, and R. Garnett (Eds.), Vol. 32. Curran Associates, Inc., 9940–9950.
- Sarah Bechtel, Artem Molchanov, Yevgen Chebotar, Edward Grefenstette, Ludovic Righetti, Gaurav Sukhatme, and Franziska Meier. 2019. Meta-learning via learned loss. *arXiv preprint arXiv:1906.05374* (2019).
- Mikhail Belkin, Daniel Hsu, Siyuan Ma, and Soumik Mandal. 2019. Reconciling modern machine-learning practice and the classical bias–variance trade-off. *Proceedings of the National Academy of Sciences* 116, 32 (2019), 15849–15854.
- Guy Blanc, Neha Gupta, Gregory Valiant, and Paul Valiant. 2020. Implicit regularization for deep neural networks driven by an ornstein-uhlenbeck like process. In *Conference on Learning Theory*. 483–513.

- Pratik Chaudhari, Anna Choromanska, Stefano Soatto, Yann LeCun, Carlo Baldassi, Christian Borgs, Jennifer Chayes, Levent Sagun, and Riccardo Zecchina. 2019. Entropy-SGD: Biasing gradient descent into wide valleys. *Journal of Statistical Mechanics: Theory and Experiment* 2019, 12 (2019), 124018.
- JSR Chisholm. 1973. Rational approximants defined from double power series. *Math. Comp.* 27, 124 (1973), 841–848.
- Terrance DeVries and Graham W Taylor. 2017. Improved regularization of convolutional neural networks with cutout. *arXiv preprint arXiv:1708.04552* (2017).
- Joseph BJ Fourier. 1829. La théorie analytique de la chaleur. *Mémoires de l'Académie Royale des Sciences de l'Institut de France* 8 (1829), 581–622.
- Aditya Sharad Golatkar, Alessandro Achille, and Stefano Soatto. 2019. Time Matters in Regularizing Deep Networks: Weight Decay and Data Augmentation Affect Early Learning Dynamics, Matter Little Near Convergence. In *Advances in Neural Information Processing Systems* 32. 10677–10687.
- Santiago Gonzalez and Risto Miikkulainen. 2020. Improved Training Speed, Accuracy, and Data Utilization Through Loss Function Optimization. In *Proceedings of the IEEE Congress on Evolutionary Computation (CEC)*.
- Santiago Gonzalez and Risto Miikkulainen. 2021. Optimizing Loss Functions Through Multivariate Taylor Polynomial Parameterization. *Proceedings of the Genetic and Evolutionary Computation Conference (GECCO-2021)* (07 2021).
- Ian J Goodfellow, Jonathon Shlens, and Christian Szegedy. 2015. Explaining and harnessing adversarial examples. In *Third International Conference on Learning Representations (ICLR)*.
- PR Graves-Morris. 1979. The numerical calculation of Padé approximants. In *Padé approximation and its applications*. Springer, 231–245.
- PR Graves-Morris and DE Roberts. 1975. Calculation of Canterbury approximants. *Computer Physics Communications* 10, 4 (1975), 234–244.
- John J Grefenstette and J Michael Fitzpatrick. 1985. Genetic search with approximate function evaluations. In *Proceedings of an International Conference on Genetic Algorithms and Their Applications*. 112–120.
- Nikolaus Hansen and Stefan Kern. 2004. Evaluating the CMA evolution strategy on multimodal test functions. In *International Conference on Parallel Problem Solving from Nature*. Springer, 282–291.
- Nikolaus Hansen and Andreas Ostermeier. 1996. Adapting arbitrary normal mutation distributions in evolution strategies: The covariance matrix adaptation. In *Proceedings of IEEE international conference on evolutionary computation*. IEEE, 312–317.
- Nikolaus Hansen and Andreas Ostermeier. 2001. Completely derandomized self-adaptation in evolution strategies. *Evolutionary computation* 9, 2 (2001), 159–195.
- Stephen José Hanson and Lorien Y Pratt. 1989. Comparing biases for minimal network construction with back-propagation. In *Advances in Neural Information Processing Systems*. 177–185.
- Kaiming He, Xiangyu Zhang, Shaoqing Ren, and Jian Sun. 2016. Identity mappings in deep residual networks. In *European conference on computer vision*. Springer, 630–645.
- Rein Houthoofd, Yuhua Chen, Phillip Isola, Bradly Stadie, Filip Wolski, OpenAI Jonathan Ho, and Pieter Abbeel. 2018. Evolved policy gradients. In *Advances in Neural Information Processing Systems* 31. 5400–5409.
- Sergey Ioffe and Christian Szegedy. 2015. Batch Normalization: Accelerating Deep Network Training by Reducing Internal Covariate Shift. In *International Conference on Machine Learning*. 448–456.
- Takashi Ishida, Ikko Yamane, Tomoya Sakai, Gang Niu, and Masashi Sugiyama. 2020. Do We Need Zero Training Loss After Achieving Zero Training Error? *arXiv preprint arXiv:2002.08709* (2020).
- Yaochu Jin. 2011. Surrogate-assisted evolutionary computation: Recent advances and future challenges. *Swarm and Evolutionary Computation* 1 (06 2011), 61–70. <https://doi.org/10.1016/j.swevo.2011.05.001>
- Nitish Shirish Keskar, Dheevatsa Mudigere, Jorge Nocedal, Mikhail Smelyanskiy, and Ping Tak Peter Tang. 2017. On large-batch training for deep learning: Generalization gap and sharp minima. In *Proceedings of the Fifth International Conference on Learning Representations (ICLR)*.
- Alex Krizhevsky and Geoffrey Hinton. 2009. *Learning multiple layers of features from tiny images*. Technical Report. University of Toronto.
- Alex Krizhevsky, Ilya Sutskever, and Geoffrey E Hinton. 2012. ImageNet Classification with Deep Convolutional Neural Networks. In *Advances in Neural Information Processing Systems 25*, F. Pereira, C. J. C. Burges, L. Bottou, and K. Q. Weinberger (Eds.). Curran Associates, Inc., 1097–1105.
- Hao Li, Zheng Xu, Gavin Taylor, Christoph Studer, and Tom Goldstein. 2018. Visualizing the Loss Landscape of Neural Nets. In *Advances in Neural Information Processing Systems 31*, S. Bengio, H. Wallach, H. Larochelle, K. Grauman, N. Cesa-Bianchi, and R. Garnett (Eds.). Curran Associates, Inc., 6389–6399.
- Yuanzhi Li, Colin Wei, and Tengyu Ma. 2019. Towards Explaining the Regularization Effect of Initial Large Learning Rate in Training Neural Networks. In *Advances in Neural Information Processing Systems 32*, H. Wallach, H. Larochelle, A. Beygelzimer, F. d'Alché-Buc, E. Fox, and R. Garnett (Eds.). Curran Associates, Inc., 11674–11685.

- Luke Metz, Niru Maheswaranathan, Brian Cheung, and Jascha Sohl-Dickstein. 2018. Meta-Learning Update Rules for Unsupervised Representation Learning. In *International Conference on Learning Representations*.
- Nelson Morgan and Hervé Bourlard. 1990. Generalization and parameter estimation in feedforward nets: Some experiments. In *Advances in Neural Information Processing Systems*. 630–637.
- Kristen Morse, Neha Das, Yixin Lin, Austin Wang, Akshara Rai, and Franziska Meier. 2020. Learning State-Dependent Losses for Inverse Dynamics Learning. *arXiv preprint arXiv:2003.04947* (2020).
- Preetum Nakkiran, Gal Kaplun, Yamini Bansal, Tristan Yang, Boaz Barak, and Ilya Sutskever. 2019. Deep Double Descent: Where Bigger Models and More Data Hurt. In *International Conference on Learning Representations (ICLR)*.
- Behnam Neyshabur, Russ R Salakhutdinov, and Nati Srebro. 2015. Path-SGD: Path-Normalized Optimization in Deep Neural Networks. In *Advances in Neural Information Processing Systems 28*, C. Cortes, N. D. Lawrence, D. D. Lee, M. Sugiyama, and R. Garnett (Eds.). Curran Associates, Inc., 2422–2430.
- Behnam Neyshabur, Ryota Tomioka, Ruslan Salakhutdinov, and Nathan Srebro. 2017. Geometry of optimization and implicit regularization in deep learning. *arXiv preprint arXiv:1705.03071* (2017).
- Scott Niekum, Andrew G Barto, and Lee Spector. 2010. Genetic programming for reward function search. *IEEE Transactions on Autonomous Mental Development* 2, 2 (2010), 83–90.
- Lee Spector, Erik Goodman, A Wu, W B. Langdon, H m. Voigt, M Gen, S Sen, M Dorigo, S Pezeshk, M Garzon, E Burke, and Morgan Kaufmann Publishers. 2001. Autoconstructive Evolution: Push, PushGP, and Pushpop. *Proceedings of the Genetic and Evolutionary Computation Conference (GECCO-2001)* (05 2001).
- Jost Tobias Springenberg, Alexey Dosovitskiy, Thomas Brox, and Martin A. Riedmiller. 2015. Striving for Simplicity: The All Convolutional Net. *CoRR abs/1412.6806* (2015).
- Nitish Srivastava, Geoffrey Hinton, Alex Krizhevsky, Ilya Sutskever, and Ruslan Salakhutdinov. 2014. Dropout: a simple way to prevent neural networks from overfitting. *The Journal of Machine Learning Research JMLR* 15, 1 (2014), 1929–1958.
- Flood Sung, Li Zhang, Tao Xiang, Timothy Hospedales, and Yongxin Yang. 2017. Learning to learn: Meta-critic networks for sample efficient learning. *arXiv preprint arXiv:1706.09529* (2017).
- C. Szegedy, V. Vanhoucke, S. Ioffe, J. Shlens, and Z. Wojna. 2016. Rethinking the Inception Architecture for Computer Vision. In *2016 IEEE Conference on Computer Vision and Pattern Recognition (CVPR)*. 2818–2826.
- Brook Taylor. 1715. *Methodus incrementorum directa & inversa*. Auctore Brook Taylor, LL. D. & Regiae Societatis Secretario. typis Pearsonianis: prostant apud Gul. Innys ad Insignia Principis.
- Henry Wilbraham. 1848. On a certain periodic function. *The Cambridge and Dublin Mathematical Journal* 3 (1848), 198–201.
- Ashia C Wilson, Rebecca Roelofs, Mitchell Stern, Nati Srebro, and Benjamin Recht. 2017. The Marginal Value of Adaptive Gradient Methods in Machine Learning. In *Advances in Neural Information Processing Systems 30*, I. Guyon, U. V. Luxburg, S. Bengio, H. Wallach, R. Fergus, S. Vishwanathan, and R. Garnett (Eds.). Curran Associates, Inc., 4148–4158.
- Yuan Yao, Lorenzo Rosasco, and Andrea Caponnetto. 2007. On early stopping in gradient descent learning. *Constructive Approximation* 26, 2 (2007), 289–315.
- Sangdoon Yun, Dongyoon Han, Seong Joon Oh, Sanghyuk Chun, Junsuk Choe, and Youngjoon Yoo. 2019. CutMix: Regularization strategy to train strong classifiers with localizable features. In *Proceedings of the IEEE International Conference on Computer Vision (ICCV)*. 6023–6032.
- Sergey Zagoruyko and Nikos Komodakis. 2016. Wide residual networks. *arXiv preprint arXiv:1605.07146* (2016).
- Hongyi Zhang, Moustapha Cisse, Yann N Dauphin, and David Lopez-Paz. 2018. mixup: Beyond Empirical Risk Minimization. In *International Conference on Learning Representations (ICLR)*.
- Wei Zhou, Yiyang Li, Yongxin Yang, Huaimin Wang, and Timothy M Hospedales. 2020. Online Meta-Critic Learning for Off-Policy Actor-Critic Methods. *arXiv preprint arXiv:2003.05334* (2020).

A NOTATION OVERVIEW

Symbol	Description
$h(\mathbf{x}_i, \boldsymbol{\theta})$	The model, with a softmax
$h_k(\mathbf{x}_i, \boldsymbol{\theta})$	The model's k th scaled logit
$D_j(f)$	The directional derivative of f along j
\mathbb{P}_{data}	Probability distribution of original data
\mathbf{x}_i	An input data sample, where $\mathbf{x}_i \sim \mathbb{P}_{\text{data}}$
\mathbf{y}_i	A label that corresponds to the \mathbf{x}_i sample
η	Learning rate
n	Number of classes
$\boldsymbol{\theta}$	A model's trainable parameters
$\boldsymbol{\lambda}$	The loss function's parameters
$\mathcal{L}(\mathbf{x}_i, \mathbf{y}_i, \boldsymbol{\theta})$	The loss function
$\gamma_k(\mathbf{x}_i, \mathbf{y}_i, \boldsymbol{\theta})$	Decomposed loss function expression from Equation 9

B BAIKAL ATTRACTORS

Theorem 1: Zero training error regions of the weight space are not attractors for the Baikal loss function.

Proof: Given that Baikal does tend to minimize training error to a large degree—otherwise it would be useless as a loss function since we are effectively assuming that the training data is in-distribution—we can observe what happens as we approach a point in parameter space that is arbitrarily-close to zero training error. Assume, without loss of generality, that all non-target scaled logits have the same value.

$$\theta_j \leftarrow \theta_j + \eta \frac{1}{n} \sum_{k=1}^n \begin{cases} \lim_{h_k(\mathbf{x}_i, \boldsymbol{\theta}) \rightarrow \frac{\epsilon}{n-1}} \gamma_k(\mathbf{x}_i, \mathbf{y}_i, \boldsymbol{\theta}) D_j(h_k(\mathbf{x}_i, \boldsymbol{\theta})) & y_{ik} = 0 \\ \lim_{h_k(\mathbf{x}_i, \boldsymbol{\theta}) \rightarrow 1-\epsilon} \gamma_k(\mathbf{x}_i, \mathbf{y}_i, \boldsymbol{\theta}) D_j(h_k(\mathbf{x}_i, \boldsymbol{\theta})) & y_{ik} = 1 \end{cases} \quad (42)$$

$$= \theta_j + \eta \frac{1}{n} \sum_{k=1}^n \begin{cases} \lim_{h_k(\mathbf{x}_i, \boldsymbol{\theta}) \rightarrow \frac{\epsilon}{n-1}} \left(\frac{1}{h_k(\mathbf{x}_i, \boldsymbol{\theta})} + \frac{0}{h_k(\mathbf{x}_i, \boldsymbol{\theta})^2} \right) D_j(h_k(\mathbf{x}_i, \boldsymbol{\theta})) & y_{ik} = 0 \\ \lim_{h_k(\mathbf{x}_i, \boldsymbol{\theta}) \rightarrow 1-\epsilon} \left(\frac{1}{h_k(\mathbf{x}_i, \boldsymbol{\theta})} + \frac{1}{h_k(\mathbf{x}_i, \boldsymbol{\theta})^2} \right) D_j(h_k(\mathbf{x}_i, \boldsymbol{\theta})) & y_{ik} = 1 \end{cases} \quad (43)$$

$$= \theta_j + \eta \frac{1}{n} \sum_{k=1}^n \begin{cases} \frac{n-1}{\epsilon} D_j(h_k(\mathbf{x}_i, \boldsymbol{\theta})) & y_{ik} = 0 \\ \left(\frac{1}{1-\epsilon} + \frac{1}{(1-\epsilon)^2} \right) D_j(h_k(\mathbf{x}_i, \boldsymbol{\theta})) & y_{ik} = 1 \end{cases} \quad (44)$$

$$= \theta_j + \eta \frac{1}{n} \sum_{k=1}^n \begin{cases} \frac{n-1}{\epsilon} D_j(h_k(\mathbf{x}_i, \boldsymbol{\theta})) & y_{ik} = 0 \\ \frac{2-\epsilon}{\epsilon^2 - 2\epsilon + 1} D_j(h_k(\mathbf{x}_i, \boldsymbol{\theta})) & y_{ik} = 1 \end{cases} \quad (45)$$

The behavior in the $y_{ik} = 0$ case will dominate for small values of ϵ . Both cases have a positive range for small values of ϵ , ultimately resulting in non-target scaled logits becoming maximized, and subsequently the non-target logit becoming minimized. This is equivalent, in expectation, to saying that ϵ will become larger after applying the learning rule. A larger ϵ clearly implies a move

away from a zero training error area of the parameter space. Thus, zero training error is not an attractor for the Baikal loss function. \square

C CHANGE IN ENTROPY

Theorem 2. The change in entropy is proportional to

$$\frac{\epsilon(\epsilon - 1) \left(e^{\epsilon(\epsilon-1)(\gamma_{-T}-\gamma_T)} - e^{\frac{\epsilon(\epsilon-1)\gamma_T(n-1)+\epsilon\gamma_{-T}(\epsilon(n-3)+n-1)}{(n-1)^2}} \right)}{(\epsilon - 1) e^{\epsilon(\epsilon-1)(\gamma_{-T}-\gamma_T)} - \epsilon e^{\frac{\epsilon(\epsilon-1)\gamma_T(n-1)+\epsilon\gamma_{-T}(\epsilon(n-3)+n-1)}{(n-1)^2}}}, \quad (46)$$

where γ_{-T} is the value of γ_j for non-target logits, and γ_T for the target logit.

Proof: Let us analyze the case where all non-target logits have the same value, $\frac{\epsilon}{n-1}$, and the target logit has the value $1 - \epsilon$. That is, all non-target classes have equal probabilities.

A model's scaled logit for an input \mathbf{x}_i can be represented as:

$$h_k(\mathbf{x}_i, \boldsymbol{\theta}) = \sigma_k(f(\mathbf{x}_i, \boldsymbol{\theta})) = \frac{e^{f_k(\mathbf{x}_i, \boldsymbol{\theta})}}{\sum_{j=1}^n e^{f_j(\mathbf{x}_i, \boldsymbol{\theta})}} \quad (47)$$

where $f_k(\mathbf{x}_i, \boldsymbol{\theta})$ is a raw output logit from the model.

The (k, j) th entry of the Jacobian matrix for $h(\mathbf{x}_i, \boldsymbol{\theta})$ can be easily derived through application of the chain rule:

$$J_{kj}h(\mathbf{x}_i, \boldsymbol{\theta}) = \frac{\partial h_k(\mathbf{x}_i, \boldsymbol{\theta})}{\partial f_j(\mathbf{x}_i, \boldsymbol{\theta})} = \begin{cases} h_j(\mathbf{x}_i, \boldsymbol{\theta}) (1 - h_k(\mathbf{x}_i, \boldsymbol{\theta})) f_k(\mathbf{x}_i, \boldsymbol{\theta}) & k = j \\ -h_j(\mathbf{x}_i, \boldsymbol{\theta}) h_k(\mathbf{x}_i, \boldsymbol{\theta}) f_k(\mathbf{x}_i, \boldsymbol{\theta}) & k \neq j \end{cases} \quad (48)$$

Consider an SGD learning rule of the form:

$$\theta_j \leftarrow \theta_j + \eta \frac{1}{n} \sum_{k=1}^n [\gamma_k(\mathbf{x}_i, \mathbf{y}_i, \boldsymbol{\theta}) D_j(h_k(\mathbf{x}_i, \boldsymbol{\theta}))] \quad (49)$$

Let us freeze a network at any specific point during the training process for any specific sample. Now, treating all $f_j(\mathbf{x}_i, \boldsymbol{\theta})$, $j \in [1, n]$ as free parameters with unit derivatives, rather than as functions. That is, $\theta_j \propto f_j(\mathbf{x}_i, \boldsymbol{\theta})$. We observe that updates are as follows:

$$\Delta f_j \propto \sum_{k=1}^n \gamma_j \begin{cases} h_j(\mathbf{x}_i, \boldsymbol{\theta}) (1 - h_k(\mathbf{x}_i, \boldsymbol{\theta})) & k = j \\ -h_j(\mathbf{x}_i, \boldsymbol{\theta}) h_k(\mathbf{x}_i, \boldsymbol{\theta}) & k \neq j \end{cases} \quad (50)$$

For downstream analysis, we can consider, as substitutions for γ_j above, γ_{-T} to be the value for non-target logits, and γ_T for the target logit.

This sum can be expanded and conceptually simplified by considering j indices and $\neg j$ indices. $\neg j$ indices, of which there are $n - 1$, are either all non-target logits, or one is the target logit in the case where j is not the target logit. Let us consider both cases, while substituting the scaled logit values defined above:

$$\Delta f_j \propto \begin{cases} \gamma_{-T} \sum_{k \neq j} h(\mathbf{x}_i, \boldsymbol{\theta}) + (n - 2)\gamma_{-T} \sum_{k \neq j} h(\mathbf{x}_i, \boldsymbol{\theta}) + \gamma_T \sum_{k \neq j} h(\mathbf{x}_i, \boldsymbol{\theta}) & \text{non-target } j \\ \gamma_T \sum_{k=j} h(\mathbf{x}_i, \boldsymbol{\theta}) + (n - 1)\gamma_{-T} \sum_{k \neq j} h(\mathbf{x}_i, \boldsymbol{\theta}) & \text{target } j \end{cases} \quad (51)$$

$$\Delta f_j \propto \begin{cases} \begin{aligned} &\gamma_{-T} h_{-T}(\mathbf{x}_i, \boldsymbol{\theta}) (1 - h_{-T}(\mathbf{x}_i, \boldsymbol{\theta})) \\ &+ (n-2) \gamma_{-T} (-h_{-T}(\mathbf{x}_i, \boldsymbol{\theta}) h_{-T}(\mathbf{x}_i, \boldsymbol{\theta})) \\ &\quad + \gamma_T (-h_{-T}(\mathbf{x}_i, \boldsymbol{\theta}) h_T(\mathbf{x}_i, \boldsymbol{\theta})) \end{aligned} & \text{non-target } j \\ \begin{aligned} &\gamma_T h_T(\mathbf{x}_i, \boldsymbol{\theta}) (1 - h_T(\mathbf{x}_i, \boldsymbol{\theta})) \\ &+ (n-1) \gamma_{-T} (-h_{-T}(\mathbf{x}_i, \boldsymbol{\theta}) h_T(\mathbf{x}_i, \boldsymbol{\theta})) \end{aligned} & \text{target } j \end{cases} \quad (52)$$

$$\text{where } h_T(\mathbf{x}_i, \boldsymbol{\theta}) = 1 - \epsilon, \quad h_{-T}(\mathbf{x}_i, \boldsymbol{\theta}) = \frac{\epsilon}{n-1} \quad (53)$$

$$\Delta f_j \propto \begin{cases} \gamma_{-T} \frac{\epsilon}{n-1} \left(1 - \frac{\epsilon}{n-1}\right) + \gamma_{-T} (n-2) \frac{\epsilon^2}{n^2 - 2n + 1} + \gamma_T (\epsilon - 1) \frac{\epsilon}{n-1} & \text{non-target } j \\ \gamma_T \epsilon - \gamma_T \epsilon^2 + \gamma_{-T} (n-1) (\epsilon - 1) \frac{\epsilon}{n-1} & \text{target } j \end{cases} \quad (54)$$

At this point, we have closed-form solutions for the changes to softmax inputs. To characterize entropy, we must now derive solutions for the changes to softmax outputs given such changes to the inputs. That is:

$$\Delta \sigma_j(f(\mathbf{x}_i, \boldsymbol{\theta})) = \frac{e^{f_j(\mathbf{x}_i, \boldsymbol{\theta}) + \Delta f_j}}{\sum_{k=1}^n e^{f_k(\mathbf{x}_i, \boldsymbol{\theta}) + \Delta f_k}} \quad (55)$$

Due to the two cases in Δf_j , $\Delta \sigma_j(f(\mathbf{x}_i, \boldsymbol{\theta}))$ is thus also split into two cases for target and non-target logits:

$$\Delta \sigma_j(f(\mathbf{x}_i, \boldsymbol{\theta})) = \begin{cases} \frac{e^{f_{-T}(\mathbf{x}_i, \boldsymbol{\theta}) + \Delta f_{-T}}}{(n-1)e^{f_{-T}(\mathbf{x}_i, \boldsymbol{\theta}) + \Delta f_{-T}} + e^{f_T(\mathbf{x}_i, \boldsymbol{\theta}) + \Delta f_T}} & \text{non-target } j \\ \frac{e^{f_T(\mathbf{x}_i, \boldsymbol{\theta}) + \Delta f_T}}{(n-1)e^{f_{-T}(\mathbf{x}_i, \boldsymbol{\theta}) + \Delta f_{-T}} + e^{f_T(\mathbf{x}_i, \boldsymbol{\theta}) + \Delta f_T}} & \text{target } j \end{cases} \quad (56)$$

Now, we can see that scaled logits have a lower entropy distribution when $\Delta \sigma_T(f(\mathbf{x}_i, \boldsymbol{\theta})) > 0$ and $\Delta \sigma_{-T}(f(\mathbf{x}_i, \boldsymbol{\theta})) < 0$. Essentially, the target and non-target scaled logits are being repelled from each other. We can ignore either of these inequalities, if one is satisfied then both are satisfied, in part because $|\sigma(f(\mathbf{x}_i, \boldsymbol{\theta}))|_1 = 1$. The target-case constraint (i.e., the target scaled logit must grow) can be represented as:

$$\frac{e^{f_T(\mathbf{x}_i, \boldsymbol{\theta}) + \Delta f_T}}{(n-1)e^{f_{-T}(\mathbf{x}_i, \boldsymbol{\theta}) + \Delta f_{-T}} + e^{f_T(\mathbf{x}_i, \boldsymbol{\theta}) + \Delta f_T}} > 1 - \epsilon \quad (57)$$

Consider the target logit case prior to changes:

$$\frac{e^{f_T(\mathbf{x}_i, \boldsymbol{\theta})}}{(n-1)e^{f_{-T}(\mathbf{x}_i, \boldsymbol{\theta})} + e^{f_T(\mathbf{x}_i, \boldsymbol{\theta})}} = 1 - \epsilon \quad (58)$$

Let us solve for $e^{f_T(\mathbf{x}_i, \boldsymbol{\theta})}$:

$$e^{f_T(\mathbf{x}_i, \boldsymbol{\theta})} = (n-1)e^{f_{-T}(\mathbf{x}_i, \boldsymbol{\theta})} + e^{f_T(\mathbf{x}_i, \boldsymbol{\theta})} - \epsilon(n-1)e^{f_{-T}(\mathbf{x}_i, \boldsymbol{\theta})} - \epsilon e^{f_T(\mathbf{x}_i, \boldsymbol{\theta})} \quad (59)$$

$$= \left(\frac{n-1}{\epsilon} - n + 1\right) e^{f_{-T}(\mathbf{x}_i, \boldsymbol{\theta})} \quad (60)$$

Substituting this definition into Equation 57:

$$\frac{e^{\Delta f_T} \left(\frac{n-1}{\epsilon} - n + 1\right) e^{f_{-T}(\mathbf{x}_i, \boldsymbol{\theta})}}{(n-1)e^{f_{-T}(\mathbf{x}_i, \boldsymbol{\theta}) + \Delta f_{-T}} + e^{\Delta f_T} \left(\frac{n-1}{\epsilon} - n + 1\right) e^{f_{-T}(\mathbf{x}_i, \boldsymbol{\theta})}} > 1 - \epsilon \quad (61)$$

Coalescing exponents:

$$\frac{e^{\Delta f_T + f_{-T}(\mathbf{x}_i, \boldsymbol{\theta})} \left(\frac{n-1}{\epsilon} - n + 1 \right)}{(n-1)e^{f_{-T}(\mathbf{x}_i, \boldsymbol{\theta}) + \Delta f_{-T}} + e^{\Delta f_T + f_{-T}(\mathbf{x}_i, \boldsymbol{\theta})} \left(\frac{n-1}{\epsilon} - n + 1 \right)} + \epsilon - 1 > 0 \quad (62)$$

Substituting in definitions for Δf_T and Δf_{-T} and greatly simplifying in a CAS is able to remove instances of f_{-T} :

$$\frac{\epsilon(\epsilon-1) \left(e^{\epsilon(\epsilon-1)(\gamma_{-T}-\gamma_T)} - e^{\frac{\epsilon(\epsilon-1)\gamma_T(n-1) + \epsilon\gamma_{-T}(\epsilon(n-3) + n-1)}{(n-1)^2}} \right)}{(\epsilon-1)e^{\epsilon(\epsilon-1)(\gamma_{-T}-\gamma_T)} - \epsilon e^{\frac{\epsilon(\epsilon-1)\gamma_T(n-1) + \epsilon\gamma_{-T}(\epsilon(n-3) + n-1)}{(n-1)^2}}} > 0 \quad (63)$$

□

D IMPLICIT LABEL SMOOTHING

Theorem 3. For any λ and any $\alpha \in (0, 1)$, there exists a $\hat{\lambda}$ such that the behavior imposed by $\hat{\lambda}$ without explicit label smoothing is identical to the behavior imposed by λ with explicit label smoothing.

Proof: Consider a basic setup with standard label smoothing, controlled by a hyperparameter $\alpha \in (0, 1)$, such that the target value in any \mathbf{y}_i is $1 - \alpha \frac{n-1}{n}$, rather than 1, and non-target values are $\frac{\alpha}{n}$, rather than 0. The learning rule changes in the general case as follows:

$$\gamma_k(\mathbf{x}_i, \mathbf{y}_i, \boldsymbol{\theta}) = \begin{cases} c_1 + c_h h_k(\mathbf{x}_i, \boldsymbol{\theta}) + c_{hh} h_k(\mathbf{x}_i, \boldsymbol{\theta})^2 \\ + c_{hy} h_k(\mathbf{x}_i, \boldsymbol{\theta}) \frac{\alpha}{n} + c_y \frac{\alpha}{n} + c_{yy} \frac{\alpha^2}{n^2} & y_{ik} = 0 \\ c_1 + c_h h_k(\mathbf{x}_i, \boldsymbol{\theta}) + c_{hh} h_k(\mathbf{x}_i, \boldsymbol{\theta})^2 + c_{hy} h_k(\mathbf{x}_i, \boldsymbol{\theta}) \left(1 - \alpha \frac{n-1}{n} \right) \\ + c_y \left(1 - \alpha \frac{n-1}{n} \right) + c_{yy} \left(1 - \alpha \frac{n-1}{n} \right)^2 & y_{ik} = 1 \end{cases} \quad (64)$$

Let $\hat{c}_1, \hat{c}_h, \hat{c}_{hh}, \hat{c}_{hy}, \hat{c}_y, \hat{c}_{yy}$ represent settings for $c_1, c_h, c_{hh}, c_{hy}, c_y, c_{yy}$ in the non-label-smoothed case that implicitly apply label smoothing within the TaylorGLO parameterization. Given the two cases in the label-smoothed and non-label-smoothed definitions of $\gamma_k(\mathbf{x}_i, \mathbf{y}_i, \boldsymbol{\theta})$, there are two equations that must be satisfiable by settings of \hat{c} constants for any c constants, with shared terms highlighted in blue and red:

$$\begin{aligned} & c_1 + c_h h_k(\mathbf{x}_i, \boldsymbol{\theta}) + c_{hh} h_k(\mathbf{x}_i, \boldsymbol{\theta})^2 + c_{hy} h_k(\mathbf{x}_i, \boldsymbol{\theta}) \frac{\alpha}{n} + c_y \frac{\alpha}{n} + c_{yy} \frac{\alpha^2}{n^2} \\ & = \hat{c}_1 + \hat{c}_h h_k(\mathbf{x}_i, \boldsymbol{\theta}) + \hat{c}_{hh} h_k(\mathbf{x}_i, \boldsymbol{\theta})^2 \end{aligned} \quad (65)$$

$$\begin{aligned}
 & c_1 + c_h h_k(\mathbf{x}_i, \boldsymbol{\theta}) + c_{hh} h_k(\mathbf{x}_i, \boldsymbol{\theta})^2 + c_{hy} h_k(\mathbf{x}_i, \boldsymbol{\theta}) \left(1 - \alpha \frac{n-1}{n}\right) \\
 & \quad + c_y \left(1 - \alpha \frac{n-1}{n}\right) + c_{yy} \left(1 - \alpha \frac{n-1}{n}\right)^2 \\
 & = \hat{c}_1 + \hat{c}_h h_k(\mathbf{x}_i, \boldsymbol{\theta}) + \hat{c}_{hh} h_k(\mathbf{x}_i, \boldsymbol{\theta})^2 + \hat{c}_{hy} h_k(\mathbf{x}_i, \boldsymbol{\theta}) + \hat{c}_y + \hat{c}_{yy}
 \end{aligned} \tag{66}$$

Let us then factor the left-hand side of Equation 65 in terms of different powers of $h_k(\mathbf{x}_i, \boldsymbol{\theta})$:

$$\underbrace{\left(c_1 + c_y \frac{\alpha}{n} + c_{yy} \frac{\alpha^2}{n^2}\right)}_{\hat{c}_1} + \underbrace{\left(c_h + c_{hy} \frac{\alpha}{n}\right)}_{\hat{c}_h} h_k(\mathbf{x}_i, \boldsymbol{\theta}) + \underbrace{c_{hh}}_{\hat{c}_{hh}} h_k(\mathbf{x}_i, \boldsymbol{\theta})^2 \tag{67}$$

Resulting in definitions for $\hat{c}_1, \hat{c}_h, \hat{c}_{hh}$. Let us then add the following form of zero to the left-hand side of Equation 66:

$$\left(c_{hy} h_k(\mathbf{x}_i, \boldsymbol{\theta}) \frac{\alpha}{n} + c_y \frac{\alpha}{n} + c_{yy} \frac{\alpha^2}{n^2}\right) - \left(c_{hy} h_k(\mathbf{x}_i, \boldsymbol{\theta}) \frac{\alpha}{n} + c_y \frac{\alpha}{n} + c_{yy} \frac{\alpha^2}{n^2}\right) \tag{68}$$

This allows us to substitute the definitions for $\hat{c}_1, \hat{c}_h, \hat{c}_{hh}$ from Equation 67 into Equation 66:

$$\begin{aligned}
 & \hat{c}_1 + \hat{c}_h h_k(\mathbf{x}_i, \boldsymbol{\theta}) + \hat{c}_{hh} h_k(\mathbf{x}_i, \boldsymbol{\theta})^2 - \left(c_{hy} h_k(\mathbf{x}_i, \boldsymbol{\theta}) \frac{\alpha}{n} + c_y \frac{\alpha}{n} + c_{yy} \frac{\alpha^2}{n^2}\right) \\
 & + c_{hy} h_k(\mathbf{x}_i, \boldsymbol{\theta}) \left(1 - \alpha \frac{n-1}{n}\right) + c_y \left(1 - \alpha \frac{n-1}{n}\right) + c_{yy} \left(1 - \alpha \frac{n-1}{n}\right)^2 \\
 & = \hat{c}_1 + \hat{c}_h h_k(\mathbf{x}_i, \boldsymbol{\theta}) + \hat{c}_{hh} h_k(\mathbf{x}_i, \boldsymbol{\theta})^2 + \hat{c}_{hy} h_k(\mathbf{x}_i, \boldsymbol{\theta}) + \hat{c}_y + \hat{c}_{yy}
 \end{aligned} \tag{69}$$

Simplifying into:

$$\begin{aligned}
 & c_{hy} h_k(\mathbf{x}_i, \boldsymbol{\theta}) \left(1 - \alpha \frac{n-1}{n}\right) + c_y \left(1 - \alpha \frac{n-1}{n}\right) + c_{yy} \left(1 - \alpha \frac{n-1}{n}\right)^2 \\
 & \quad - \left(c_{hy} h_k(\mathbf{x}_i, \boldsymbol{\theta}) \frac{\alpha}{n} + c_y \frac{\alpha}{n} + c_{yy} \frac{\alpha^2}{n^2}\right) \\
 & = \hat{c}_{hy} h_k(\mathbf{x}_i, \boldsymbol{\theta}) + \hat{c}_y + \hat{c}_{yy}
 \end{aligned} \tag{70}$$

Finally, factor the left-hand side of Equation 70 in terms of, $h_k(\mathbf{x}_i, \boldsymbol{\theta})$, 1, and 1^2 :

$$\begin{aligned}
 & \underbrace{\left(c_{hy} \left(1 - \alpha \frac{n-1}{n}\right) - c_{hy} \frac{\alpha}{n}\right)}_{\hat{c}_{hy}} h_k(\mathbf{x}_i, \boldsymbol{\theta}) \\
 & + \underbrace{\left(c_y \left(1 - \alpha \frac{n-1}{n}\right) - c_y \frac{\alpha}{n}\right)}_{\hat{c}_y} + \underbrace{\left(c_{yy} \left(1 - \alpha \frac{n-1}{n}\right)^2 - c_{yy} \frac{\alpha^2}{n^2}\right)}_{\hat{c}_{yy}}
 \end{aligned} \tag{71}$$

Thus, the in-parameterization constants with implicit label smoothing can be defined for any desired, label-smoothed constants as follows:

$$\hat{c}_1 = c_1 + c_y \frac{\alpha}{n} + c_{yy} \frac{\alpha^2}{n^2} \quad (72)$$

$$\hat{c}_h = c_h + c_{hy} \frac{\alpha}{n} \quad (73)$$

$$\hat{c}_{hh} = c_{hh} \quad (74)$$

$$\hat{c}_{hy} = c_{hy} \left(1 - \alpha \frac{n-1}{n}\right) - c_{hy} \frac{\alpha}{n} \quad (75)$$

$$\hat{c}_y = c_y \left(1 - \alpha \frac{n-1}{n}\right) - c_y \frac{\alpha}{n} \quad (76)$$

$$\hat{c}_{yy} = c_{yy} \left(1 - \alpha \frac{n-1}{n}\right)^2 - c_{yy} \frac{\alpha^2}{n^2} \quad (77)$$

So for any λ and any $\alpha \in (0, 1)$, there exists a $\hat{\lambda}$ such that the behavior imposed by $\hat{\lambda}$ without explicit label smoothing is identical to the behavior imposed by λ with explicit label smoothing. That is, any degree of label smoothing can be implicitly represented for any TaylorGLO loss function. \square

E TRAINABILITY OF TAYLORGLO LOSS FUNCTIONS

Theorem 4. A third-order TaylorGLO loss function is not trainable if the following constraints on λ are satisfied:

$$c_1 + c_y + c_{yy} + \frac{c_h + c_{hy}}{n} + \frac{c_{hh}}{n^2} < (n-1) \left(c_1 + \frac{c_h}{n} + \frac{c_{hh}}{n^2} \right) \quad (78)$$

$$c_y + c_{yy} + \frac{c_{hy}}{n} < (n-2) \left(c_1 + \frac{c_h}{n} + \frac{c_{hh}}{n^2} \right). \quad (79)$$

Proof: At the null epoch, a valid loss function aims to, in expectation, minimize non-target scaled logits while maximizing target scaled logits. Thus, we attempt to find cases of λ for which these behaviors occur. Considering the representation for $\gamma_k(\mathbf{x}_i, \mathbf{y}_i, \theta)$ in Equation 24:

$$\theta_j \leftarrow \theta_j + \eta \frac{1}{n} \sum_{k=1}^n \begin{cases} (c_1 + c_h h_k(\mathbf{x}_i, \theta) + c_{hh} h_k(\mathbf{x}_i, \theta)^2) D_j(h_k(\mathbf{x}_i, \theta)) & y_{ik} = 0 \\ (c_1 + c_h h_k(\mathbf{x}_i, \theta) + c_{hh} h_k(\mathbf{x}_i, \theta)^2 \\ + c_{hy} h_k(\mathbf{x}_i, \theta) + c_y + c_{yy}) D_j(h_k(\mathbf{x}_i, \theta)) & y_{ik} = 1. \end{cases} \quad (80)$$

Let us substitute $h_k(\mathbf{x}_i, \theta) = \frac{1}{n}$ (i.e., the expected value of a logit at the null epoch):

$$\theta_j \leftarrow \theta_j + \eta \frac{1}{n} \sum_{k=1}^n \begin{cases} \left(c_1 + \frac{c_h}{n} + \frac{c_{hh}}{n^2} \right) D_j(h_k(\mathbf{x}_i, \theta)) & y_{ik} = 0 \\ \left(c_1 + c_y + c_{yy} + \frac{c_h + c_{hy}}{n} + \frac{c_{hh}}{n^2} \right) D_j(h_k(\mathbf{x}_i, \theta)) & y_{ik} = 1. \end{cases} \quad (81)$$

For the desired degenerate behavior to appear, the directional derivative's coefficient in the $y_{ik} = 1$ case must be less than zero:

$$c_1 + c_y + c_{yy} + \frac{c_h + c_{hy}}{n} + \frac{c_{hh}}{n^2} < 0. \quad (82)$$

This finding can be made more general, by asserting that the directional derivative's coefficient in the $y_{ik} = 1$ case be less than $(n - 1)$ times the coefficient in the $y_{ik} = 0$ case. Thus, for a loss function to be viable it has to satisfy the following constraint on λ :

$$c_1 + c_y + c_{yy} + \frac{c_h + c_{hy}}{n} + \frac{c_{hh}}{n^2} < (n - 1) \left(c_1 + \frac{c_h}{n} + \frac{c_{hh}}{n^2} \right) \quad (83)$$

$$c_y + c_{yy} + \frac{c_{hy}}{n} < (n - 2) \left(c_1 + \frac{c_h}{n} + \frac{c_{hh}}{n^2} \right). \quad (84)$$

□